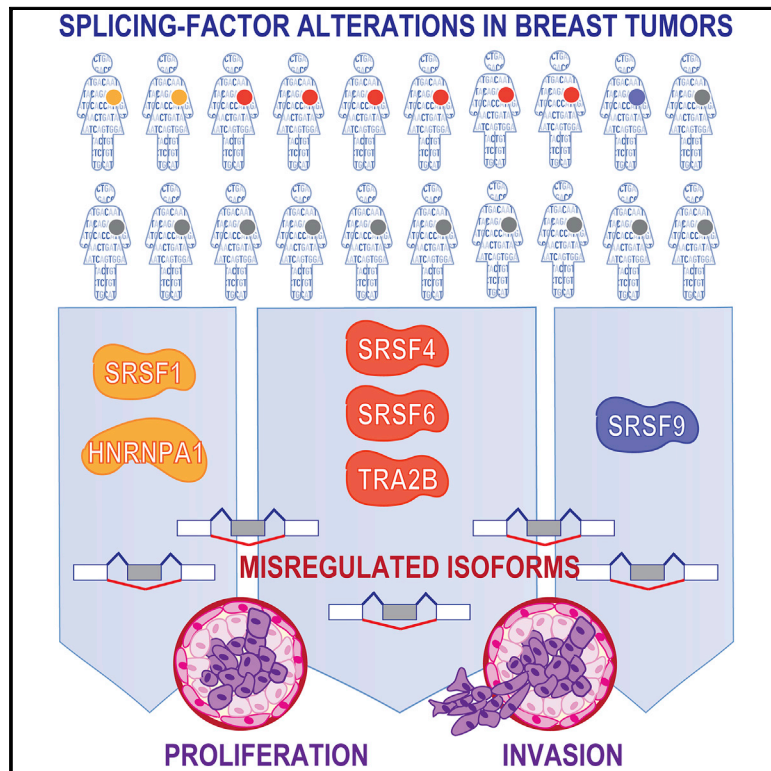


## Differential Functions of Splicing Factors in Mammary Transformation and Breast Cancer Metastasis

### Graphical Abstract



### Authors

SungHee Park, Mattia Brugiolo,  
Martin Akerman, ...,  
Senthil K. Muthuswamy,  
Adrian R. Krainer, Olga Anczuków

### Correspondence

olga.anczukow@jax.org (O.A.),  
krainer@cshl.edu (A.R.K.)

### In Brief

Park et al. demonstrate that >50% of human breast tumors exhibit an alteration in one of the splicing factors from the SR protein family. Using *in vitro* and *in vivo* breast cancer models, they identify three splicing factors that promote cell proliferation and invasion by regulating isoforms associated with cancer hallmarks.

### Highlights

- 52% of breast tumors have an alteration in at least one SR protein family member
- SRSF4, SRSF6, or TRA2 $\beta$  promotes mammary cell proliferation and invasion
- SRSF4, SRSF6, or TRA2 $\beta$  regulates shared spliced isoforms associated with cancer hallmarks
- TRA2 $\beta$  is regulated by MYC and plays a role in breast cancer metastasis



# Differential Functions of Splicing Factors in Mammary Transformation and Breast Cancer Metastasis

SungHee Park,<sup>1,8</sup> Mattia Brugiolo,<sup>1,8</sup> Martin Akerman,<sup>2,3,8</sup> Shipra Das,<sup>2,8</sup> Laura Urbanski,<sup>1,4</sup> Adam Geier,<sup>3</sup> Anil K. Kesarwani,<sup>1</sup> Martin Fan,<sup>2</sup> Nathan Leclair,<sup>1,4</sup> Kuan-Ting Lin,<sup>2</sup> Leo Hu,<sup>2</sup> Ian Hua,<sup>2</sup> Joshy George,<sup>1,5</sup> Senthil K. Muthuswamy,<sup>2,6</sup> Adrian R. Krainer,<sup>2,\*</sup> and Olga Anczuków<sup>1,2,5,7,9,\*</sup>

<sup>1</sup>The Jackson Laboratory for Genomic Medicine, Farmington, CT, USA

<sup>2</sup>Cold Spring Harbor Laboratory, Cold Spring Harbor, NY, USA

<sup>3</sup>Envisagenics Inc., New York, NY, USA

<sup>4</sup>Graduate Program in Genetics and Development, UConn Health, Farmington, CT, USA

<sup>5</sup>Institute for Systems Genomics, UConn Health, Farmington, CT, USA

<sup>6</sup>Departments of Medicine and Pathology, Beth Israel Deaconess Medical Center, Harvard Medical School, Boston, MA, USA

<sup>7</sup>Department of Genetics and Genome Sciences, UConn Health, Farmington, CT, USA

<sup>8</sup>These authors contributed equally

<sup>9</sup>Lead Contact

\*Correspondence: [olga.anczukow@jax.org](mailto:olga.anczukow@jax.org) (O.A.), [krainer@cshl.edu](mailto:krainer@cshl.edu) (A.R.K.)

<https://doi.org/10.1016/j.celrep.2019.10.110>

## SUMMARY

Misregulation of alternative splicing is a hallmark of human tumors, yet to what extent and how it contributes to malignancy are only beginning to be unraveled. Here, we define which members of the splicing factor SR and SR-like families contribute to breast cancer and uncover differences and redundancies in their targets and biological functions. We identify splicing factors frequently altered in human breast tumors and assay their oncogenic functions using breast organoid models. We demonstrate that not all splicing factors affect mammary tumorigenesis in MCF-10A cells. Specifically, the upregulation of SRSF4, SRSF6, or TRA2 $\beta$  disrupts acinar morphogenesis and promotes cell proliferation and invasion in MCF-10A cells. By characterizing the targets of these oncogenic splicing factors, we identify shared spliced isoforms associated with well-established cancer hallmarks. Finally, we demonstrate that TRA2 $\beta$  is regulated by the MYC oncogene, plays a role in metastasis maintenance *in vivo*, and its levels correlate with breast cancer patient survival.

## INTRODUCTION

Alternative RNA splicing is a key step in gene expression regulation and contributes to transcriptional diversity and plasticity by selecting which transcript isoforms are produced in a specific cell at a given time. Defects in alternative splicing (AS) are frequently found in human tumors, and RNA splicing regulators have recently emerged as a new class of oncoproteins or tumor suppressors (Dvinge et al., 2016). AS alterations can lead to malignancy by affecting the expression of oncogene and tumor-

suppressor isoforms. Tumor-associated aberrant AS profiles result from mutations in AS regulatory elements of specific cancer genes or from changes in the splicing machinery (Urbanski et al., 2018). Recurrent somatic mutations in spliceosomal components frequently occur in myeloid tumors, suggesting that splicing factor (SF) alterations are a hallmark of cancer (Yoshida and Ogawa, 2014). In solid tumors, SFs exhibit copy-number variation (CNV) and/or changes in expression level, but they are rarely mutated (Urbanski et al., 2018).

One major class of SFs is the serine/arginine-rich (SR) protein family, which acts at multiple steps of spliceosome assembly and is involved in both constitutive splicing and AS (Black, 2003). The heterogeneous nuclear ribonucleoproteins (hnRNPs) are another group of SFs that are implicated in AS regulation. SR and hnRNP A/B proteins can exhibit antagonistic effects on particular exons. Both activator and repressor SFs bind directly to pre-mRNA and elicit changes in a concentration-dependent manner (Long and Caceres, 2009); thus, changes in SF levels would likely cause AS deregulation in cancer, even in the absence of mutations, and affect a network of downstream targets. Higher SF levels increase the availability of that SF, which can bind to additional exonic or intronic target sequences and directly affect the AS of target exons by recruiting or repelling the splicing machinery (Ge and Manley, 1990; Krainer et al., 1990; Wagner et al., 2016; Zahler et al., 1993; Zhu and Krainer, 2000). Alternatively, SF binding can limit the accessibility of another RNA-binding protein (RBP) that normally would repress or activate the AS of that specific exon and thus elicit the opposite effect. Conversely, decreased SF levels will also affect the AS of its targets by limiting its ability to bind target exons and by freeing SF-binding sites, which could now be occupied by other RBPs. Although SR proteins were initially described as activators promoting exon inclusion, and hnRNPs as AS repressors, transcriptomic studies suggest that members of both families can promote inclusion for some targets and skipping for others (Bradley et al., 2015; Huelga et al., 2012).



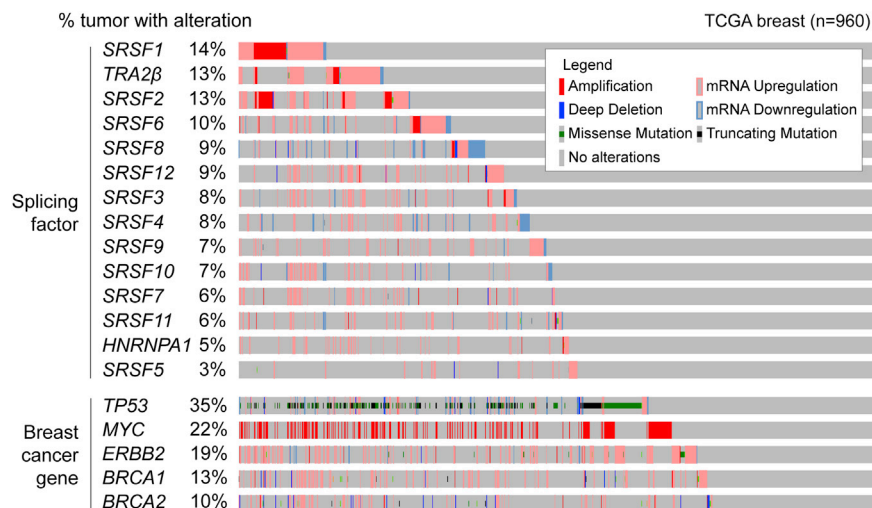


**Figure 1. SF Alterations Are Detected Frequently in Human Breast Tumors**

Graphical representation of SF alterations in TCGA human breast tumors (n = 960) sorted by frequency. CNVs and expression changes are assessed by DNA- and RNA-seq. Individual genes are represented as rows and patients as columns. Alterations in breast cancer genes *BRCA1*, *BRCA2*, *TP53*, *MYC*, and *ERBB2* are in the bottom panel.

See also Figure S1.

on the following: (1) 12 SR-protein family members, (2) the SR-like *TRA2β*, and (3) *HNRNPA1*, an *SRSF1* antagonist, reported to be misregulated in breast tumors (Karni et al., 2007; Pelisch et al., 2012). No recurrent somatic mutations in these SFs were detected in breast tumors (Table S1A). This is in contrast to

Changes in AS patterns are frequently detected in human breast tumors (Eswaran et al., 2013; Venables et al., 2008; Venables et al., 2009), yet the upstream regulators controlling these tumor-associated isoforms have not been extensively characterized. We demonstrated that the overexpression of *SRSF1*, an SF frequently upregulated in breast tumors (Karni et al., 2007), promotes the transformation of mammary cells *in vitro* and *in vivo* and acts by regulating spliced isoforms associated with proliferation and cell death (Anczuków et al., 2012, 2015). *SRSF1* is a prototypical member of the SR protein family, which comprises 12 members (*SRSF1*–*SRSF12*) with structural similarities, containing 1 or 2 RNA recognition motifs (RRMs) and a C-terminal arginine-serine-rich (RS) domain (Long and Caceres, 2009). However, little is known about differences and redundancies in their targets and biological functions in human tissues. Multiple SR proteins may play roles in breast cancer pathogenesis, as follows: (1) SR protein levels increase during murine mammary tumorigenesis (Stickeler et al., 1999), and *SRSF4*, *SRSF5*, or *SRSF6* are upregulated in human breast tumors or cell lines (Huang et al., 2007; Karni et al., 2007; Pind and Watson, 2003); (2) the increased expression of *SRSF3* correlates with tumor grade in patients (Jia et al., 2010); and (3) the SR-like protein *TRA2β* is upregulated in breast tumors (Best et al., 2013; Watermann et al., 2006). Therefore, it is critical to characterize the differences and redundancies in SR protein targets in cancer and to assess their specificities as breast oncogenes. Here, we describe the molecular portraits of SF alterations in breast tumors, focusing on the SR protein family, and identify specific SFs that promote mammary cell transformation.

## RESULTS

### Comprehensive Molecular Portrait of SF Alterations in Human Breast Tumors

We systematically assessed SF mutations, CNVs, and expression changes in 960 human breast tumors from The Cancer Genome Atlas (TCGA) dataset (Figure 1). Based on previous studies reporting SF upregulation in smaller cohorts, we focused

the recurrent *SRSF2* mutations detected in patients with myelodysplastic syndromes or chronic myelomonocytic leukemia. These findings suggest that SF mutations are not likely to play a major role in breast cancer. Nonetheless, 57% of tumors had an alteration in at least one of the SFs analyzed, revealing frequent SF CNVs and/or expression changes in breast tumors (Figure 1). Recurrent SF alterations ranged from 2% to 15% in frequency; in particular, *SRSF1*, *TRA2β*, *SRSF2*, and *SRSF6* are each altered in  $\geq 10\%$  of tumors, a substantial proportion of breast cancer patients, given that alterations in known cancer drivers *ERBB2*, *MYC*, or *TP53* are detected in 17%, 27%, and 37% of tumors, respectively (Figure 1). For many SFs, the most frequent alterations are mRNA upregulation and DNA amplification, accounting for  $>85\%$  of the total alterations detected for each SF, suggesting a selection for SF gain (Figure S1A). The two exceptions are *SRSF4* and *SRSF8*, which are downregulated in 40% and 60%, respectively, of tumors with SF alteration, and upregulated in the remaining tumors (Figure S1A). Most SFs did not show a strong correlation between CNVs and expression changes (Table S1), suggesting additional layers of regulation (e.g., at the transcriptional or the post-transcriptional level). In addition, *SRSF1*, *SRSF2*, *SRSF3*, *SRSF4*, or *TRA2β* upregulation are enriched in basal breast tumors (Figure S1B), an aggressive cancer subtype. Finally, increased *TRA2β* levels are detected in 40% of triple-negative breast cancers (TNBCs) (Figure S1C), a tumor subtype associated with poor prognosis, high metastatic incidence, and lack of effective therapies.

We investigated whether alterations in SFs co-occur with or are mutually exclusive with alterations in known cancer genes, either considering any alteration type (Table S1C) or only tumors with upregulated SFs (Table S1D). We identified 23 SF alterations co-occurring with alterations in *BRCA1*, *BRCA2*, *ERBB2*, *HRAS*, *MYC*, *PIK3CA*, or *TP53* genes (Table S1C). For example, co-occurring alterations include the following: (1) *TP53* with *SRSF3*, *SRSF12*, and *TRA2β*; (2) *HRAS* with *SRSF2*; and (3) *BRCA2* with *SRSF12* and *TRA2β* (Table S1C). Considering only upregulated SFs, (1) amplified or upregulated *MYC*

co-occurs with *SRSF1*, *SRSF3*, *SRSF4*, *SRSF7*, *SRSF12*, and *TRA2 $\beta$* ; (2) mutated *TP53* with *SRSF3*, *SRSF12*, and *TRA2 $\beta$* ; (3) amplified or upregulated *PIK3CA* with *TRA2 $\beta$* ; (4) upregulated *HRAS* with *SRSF2*, *SRSF3*, *SRSF4*, *SRSF7*, and *SRSF9*; and (5) upregulated *BRCA1* or *BRCA2* with *SRSF1*, *SRSF10*, *SRSF12*, and *TRA2 $\beta$*  (Table S1D).

Furthermore, we asked whether SF alterations were correlated with alterations in other SFs, either considering any alteration type (Table S1E) or separating amplified and upregulated SFs (Tables S1F and S1G). Of 94 possible pairs, 33 SF pairs had a tendency toward co-occurrence (Table S1E). *SRSF1* and *SRSF2* are located in a nearby region on chromosome 17, and amplifications in both genes co-occur in breast tumors (Table S1F). Other SFs located in close proximity (e.g., *SRSF3* and *SRSF12*, or *SRSF4*, *SRSF10* and *SRSF11*) do not exhibit this pattern. Focusing further on upregulated SFs (Table S1G), we identified 50 SF pairs with a tendency toward co-occurrence (e.g., *SRSF1* or *SRSF2* co-occurred with *SRSF7*, *SRSF10*, or *TRA2 $\beta$* ), whereas *TRA2 $\beta$*  co-occurred with *SRSF3*, *SRSF7*, *SRSF10*, and *SRSF12* (Table S1G). Finally, for 31 co-occurring SF alteration pairs, we detected a correlation with tumor stage (Table S1E). The strongest correlation was found for alterations in both *SRSF3* and *SRSF7*, which were enriched in T1c stage tumors.

To further determine whether defects in SF levels lead to AS alterations that could contribute to pathogenesis, we characterized the differentially spliced events (DSEs) in breast tumors with *SF-high versus SF-low* levels (Figure S2; Table S2A). AS changes were quantified using SpliceCore, commercial software that performs exon-centric AS analysis by mapping RNA sequencing (RNA-seq) data to a proprietary reference transcriptome. We combined SpliceCore results with an in-house bioinformatics pipeline based on rMATS (Shen et al., 2014) to filter and prioritize reproducible DSEs in terms of “differential percent spliced in” ( $\Delta$ PSI) scores between *SF-high versus SF-low* tumors. We focused only on DSEs detected in  $\geq 10$  tumors from both groups. For SFs frequently altered, *SRSF1*, *SRSF2*, *TRA2 $\beta$* , and *SRSF6*, we identified  $>1,000$  DSEs in *SF-high versus SF-low* tumors (Figure S2B; Tables S2B–S2O), and 27%–47% of these were detected in  $\geq 80$  tumors (Figure S2C). The most frequent type of DSEs in *SRSF1-* and *TRA2 $\beta$ -high* tumors were cassette exon (CA) (Figure S2B), equally divided between inclusion and skipping events (Figure S2D). Conversely, *SRSF6-high* tumors were enriched in included events, including in retained introns (RIs) (Figures S2B and S2D). In addition, *SRSF5-* and *SRSF11-high* tumors each displayed  $>3,000$  DSEs, but all DSEs were found in  $\leq 80$  tumors (Figures S2B and S2C), and these SF alterations were only detected in 3%–6% of tumors (Figure 1). Finally, *SRSF3-*, *SRSF9-*, *SRSF12-*, or *HNRNPA1-high* tumors displayed  $>1,000$  DSEs, but most were detected in  $\leq 80$  tumors (Figures S2B and S2C).

We conducted a pairwise comparative analysis of the 14 SF tumor groups to identify shared and unique DSEs associated with *SF-high* levels; shared DSEs had the same  $\Delta$ PSI direction (i.e., either both  $\Delta$ PSI  $\geq 10\%$  or both  $\Delta$ PSI  $\leq -10\%$ ). A total of 19 SF pairs shared between 20% and 45% of DSEs, while the remaining 72 SF pairs shared few DSEs (Table S2P). The largest overlap was detected between *SRSF3-high* and *SRSF7-high*

tumors (Table S2P). For SFs frequently altered, *SRSF1-high* tumors shared 21% of DSEs with *TRA2 $\beta$ -high* tumors and 12% with *SRSF2-high*; *TRA2 $\beta$ -high* and *SRSF2-high* tumors shared 19% of DSEs (Table S2P). In addition, to determine whether *SF-high* tumors exhibit defects in specific gene sets, we searched for shared differentially spliced genes (DSGs), defined as any DSE within the same gene regardless of the  $\Delta$ PSI direction or AS type. Here again, the largest overlap was found for *SRSF3-high* and *SRSF7-high* tumors (Table S2Q). Thus, although varying degrees of similarity and differences in AS are detected, the overall AS patterns are different in tumors with distinct SF alterations.

The finding that SFs are frequently altered in human breast tumors and are associated with the expression of distinct spliced isoforms prompted us to examine which of these SF alterations were likely to play a role in tumorigenesis.

### SF Overexpression Differentially Affects Acinar Morphogenesis and Mammary Cell Proliferation

We selected eight SFs upregulated in breast tumors to systematically determine their individual roles in mammary cell transformation. Starting with non-transformed human mammary epithelial MCF-10A cells, we generated eight derivative lines, each stably overexpressing (OE) one SF using a retroviral construct containing a T7-tagged SF cDNA or an empty vector control. Expression was confirmed by qRT-PCR, western blotting, and immunofluorescence (Figures 2A, S3A, and S3B). All T7-tagged SFs were localized primarily in the nucleus, which is consistent with their role in AS. MCF-10A cells form organized growth-arrested three-dimensional (3D) structures when grown in Matrigel, a basement-membrane-like extracellular matrix, recapitulating acinar structures from the mammary gland (Debnath and Brugge, 2005). Oncogenes associated with breast cancer disrupt the organized architecture of MCF-10A acinar structures either by affecting both acinar size and organization, thus leading to the formation of enlarged dysmorphic structures (e.g., when ERBB2 or AKT are activated [Debnath et al., 2003b; Muthuswamy et al., 2001]) or by increasing acinar size only (e.g., following cyclin D1 or MYC expression [Debnath et al., 2002; Partanen et al., 2007]). We previously showed that *SRSF1-OE* increases cell proliferation and decreases apoptosis, leading to 1.5-fold larger acini, which is indicative of transformation in MCF-10A cells (Anczuków et al., 2012). SFs were classified into three categories according to their effects on acinar morphology compared to controls: (1) *SRSF4-*, *SRSF6-*, and *TRA2 $\beta$ -OE* promoted the formation of 3- to 4-fold larger and dysmorphic acini; (2) *HNRNPA1-OE*, similarly to *SRSF1*, increased acinar size by 2-fold, but did not disrupt acinar morphology; and (3) finally, *SRSF2-*, *SRSF3-*, and *SRSF9-OE* acini were not different from controls (Figures 2B and 2C). Moreover, *SRSF6-* and *TRA2 $\beta$ -OE* led to changes in acinar size that are detectable very early during morphogenesis and increased the number of proliferating acini (Figures S3C–S3E). Overall, our findings reveal that (1) not all SFs affect oncogenic hallmarks in this model; (2) only a subset of SFs affect acinar morphogenesis or proliferation, phenotypes indicative of cellular transformation in 3D-grown MCF-10A; and (3) distinct SFs affect different cellular phenotypes indicative of transformation in MCF-10A cells, suggesting underlying

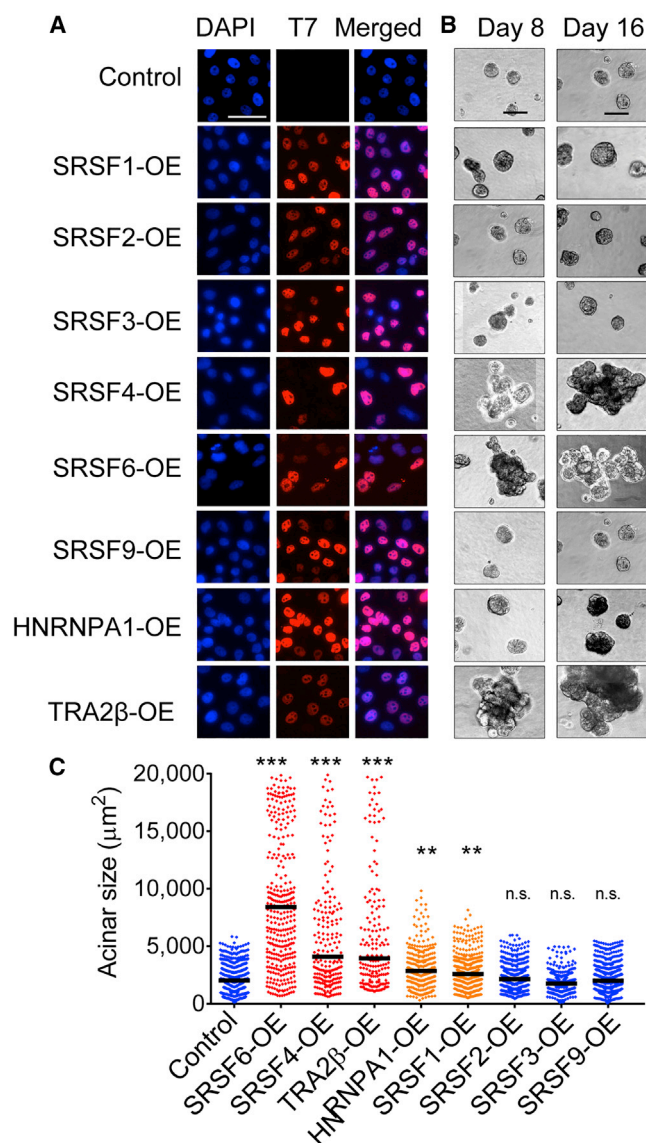


**Figure 2. Specificity of SF-Mediated Transformation**  
 (A) Expression of T7-tagged SFs in MCF-10A cells, detected by immunofluorescence using T7-tag antibody and DAPI nuclei co-stain (scale bar: 50 μm).  
 (B) Representative bright-field images of acinar size and morphology for control and SF-OE 3D MCF-10A cells on days 8 and 16 (scale bar: 100 μm).  
 (C) Quantification of acinar sizes in control and SF-OE 3D MCF-10A cells on day 16. The dot plot shows the size distribution of all of the structures and the median (horizontal line) for each condition (n = 4, >50 acini per experiment; t test, \*\*p < 0.001, \*\*\*p < 0.0001; n.s., not significant).  
 See also Figure S3.

specificities and non-redundant functions of SFs, potentially mediated by their downstream targets.

### SRSF4-, SRSF6-, and TRA2β-Regulated AS Isoforms in Breast Cancer

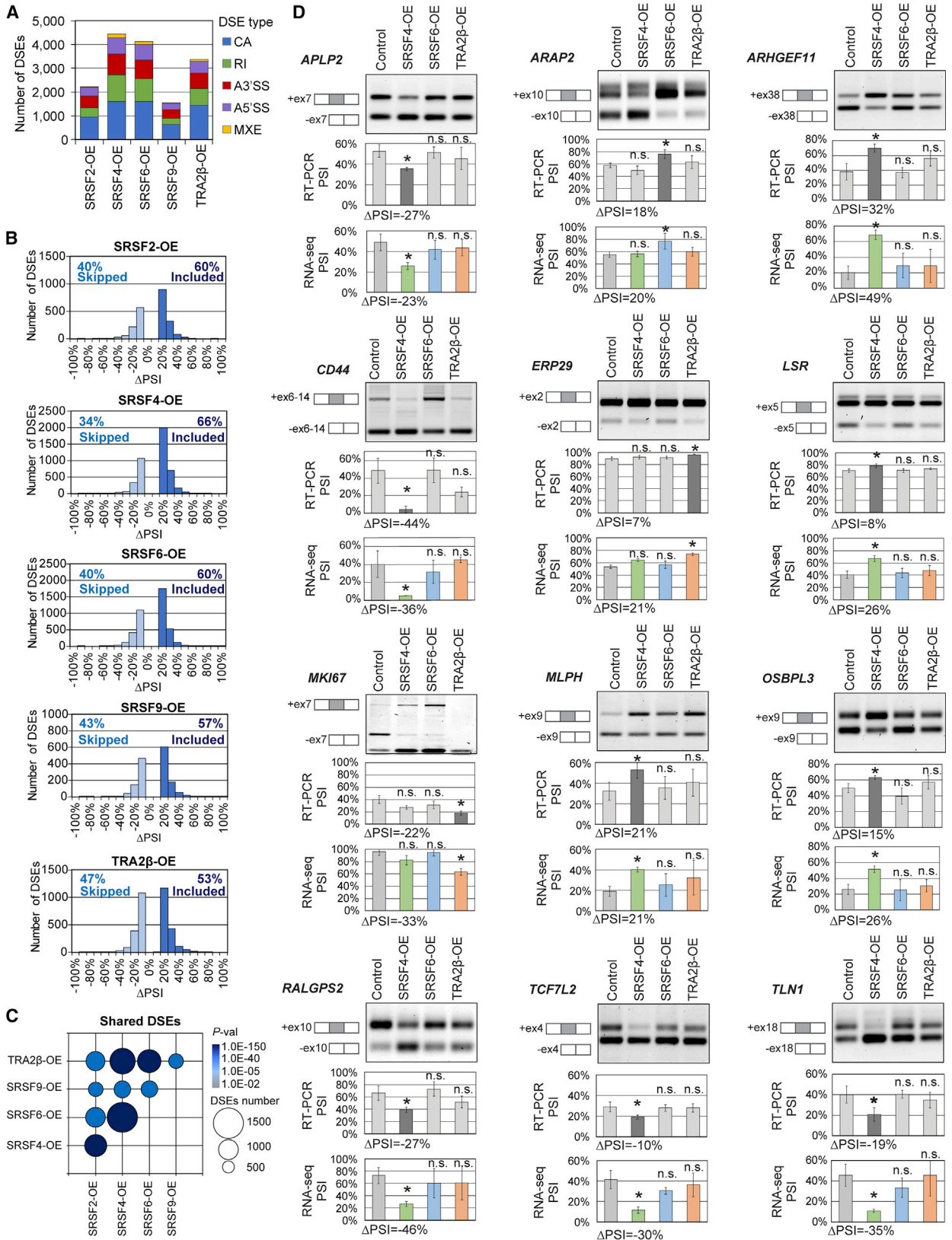
We next characterized DSEs regulated by SFs in human mammary cells and tumors, focusing especially on the targets of SRSF4, SRSF6, and TRA2β, and defined the specificity and

redundancy of these SFs. We performed RNA-seq on controls and SF-OE MCF-10A day 8 acini and identified DSEs in (1) highly proliferative and dysmorphic SRSF4-, SRSF6-, and TRA2β-OE acini and (2) SRSF2- and SRSF9-OE acini with no phenotypic difference from controls. SRSF1 targets were previously characterized by RNA-seq in MCF-10A cells (Anczuków et al., 2015) and were not investigated further here. We identified >1,500 DSEs in each condition, across multiple biological replicates (Figure 3A; Tables S3A–S3E). Almost half of these DSEs correspond to CA events, followed by RIs, alternative 5' splice sites (A5'SSs), A3'SSs, and mutually exclusive exons (MXEs) (Figure 3A). SRSF4-, SRSF6-, and TRA2β-OE acini displayed the largest number of DSEs, while SRSF2- and SRSF9-OE acini had fewer DSEs (Figure 3A). All five SFs promoted both inclusion and skipping (Figure 3B), suggesting a dual role for SR proteins as AS activators and repressors, either directly through RNA binding or indirectly through secondary interactions; this is consistent with previous findings in mice, fruit flies, and humans (Bradley et al., 2015; Pandit et al., 2013). Analysis by AS event type revealed that all five SFs promoted relatively equal numbers of inclusion and skipping CA events (Figure S4A). SRSF2-, SRSF4-, SRSF6-, and SRSF9-OE primarily promoted RI events, whereas TRA2β-OE promoted a similar number of retained and skipped introns. The majority of A5'SS and A3'SS events promoted proximal SS usage (Figure S4A). Gene set enrichment analysis revealed that SRSF4-, SRSF6-, and TRA2β-OE affect the AS of genes that regulate key cellular processes associated with transformation (Figure S4B). We then examined the overlap across all SF-OE MCF-10A datasets, either at the AS event level (Table S3F) or the gene level (Table S3G). SRSF4-, SRSF6-, and TRA2β-OE acini, which had a similar phenotype in 3D, also exhibited the greatest overlap for both DSEs and DSGs, with 30%–40% shared DSEs (Figures 3C and S4B; Tables S3F and S3G).

Next, we compared SF-driven DSEs identified in MCF-10A acini to DSEs detected in SF-high breast tumors (Tables S2B–S2O). A total of 173 DSEs were found in SRSF4-high MCF-10A acini and tumors, 96 DSEs in SRSF6-high, and 36 DSEs in TRA2β-high (Table S3I). Almost 40% of these DSEs affected regions with an annotated protein domain, suggesting that these AS alterations could produce novel protein isoforms in breast tumors.

We validated by RT-PCR 12 SF-regulated DSEs in SRSF4-, SRSF6-, and TRA2β-OE MCF-10A (Figure 3D) out of 21 randomly selected DSEs. Validated DSEs affect genes involved in proliferation (MKI67, APLP2), cell migration and adhesion (ARAP2, CD44, ERP29, LSR), signaling (ARHGEF11, MLPH, TCF7L2), or cytoskeleton organization (OSBPL3, RALGPS2, TLN1).

Since AS changes affecting protein domains are critical for protein function in cancer (Climente-González et al., 2017), we focused on DSEs that overlap protein domains and are therefore more likely to affect oncogenic phenotypes. DSEs co-occurring in SRSF4-, SRSF6-, and/or TRA2β-OE overlapped with annotated protein domains, compared to events unique to every SF (Figure S4D). In addition, to prioritize breast cancer-relevant biological processes, we selected genes associated with breast cancer based on human genetics and genomics studies in the Open Targets database (Carvalho-Silva et al., 2019). Gene set



(legend on next page)

enrichment analysis on the subset of breast cancer-associated genes with alternatively spliced protein domains revealed that SRSF4-, SRSF6-, and TRA2 $\beta$  targets, but not SRSF2 and SRSF9 targets, are enriched in cancer-relevant biological processes (Table S3K). The first three SFs are therefore likely to affect the hallmarks that are indicative of mammary transformation through protein-altering AS. DSEs detected in SRSF4-, SRSF6-, and TRA2 $\beta$ -OE acini were enriched in genes associated with cell-cycle regulation, apoptosis, Golgi-vesicle transport, and cell adhesion (Table S3K). These results suggest a pivotal role for SRSF4, SRSF6, and TRA2 $\beta$  in the splicing-regulatory network that promotes mammary transformation in MCF-10A cells, which depends at least in part on discrete and effective co-regulatory interactions with one another.

### SF-Regulated Pathways in Breast Cancer

We examined SF-induced gene expression changes in MCF-10A acini using Cuffdiff (Trapnell et al., 2013; Tables S4A–S4F). SRSF4-, SRSF6-, and TRA2 $\beta$ -OE acini exhibited the greatest number of gene expression changes, with >500 differentially expressed genes (DEGs) (Figure S4E; Tables S4B, S4C, and S4E). In contrast, SRSF2- and SRSF9-OE acini had  $\leq 40$  DEGs (Tables S4A and S4D). DEGs in SRSF4-, SRSF6-, or TRA2 $\beta$ -OE acini were enriched in targets associated with cell proliferation, migration, cytoskeleton organization, polarity, cell signaling, or cholesterol metabolism (Tables S4H–S4J). In addition, SRSF4-, SRSF6-, and TRA2 $\beta$ -OE acini shared 15%–28% of DEGs (Figure S4F; Table S4F). Shared DEGs were associated with proliferation, cell cycle, cytokine-mediated signaling, cholesterol synthesis, migration, and extracellular matrix organization (Figure S4G; Tables S4K–S4M). Thus, SRSF4, SRSF6, and TRA2 $\beta$  not only share a similar phenotype in MCF-10A cells but also regulate the expression of shared genes and spliced isoforms that affect cellular processes associated with tumor initiation and progression.

### TRA2 $\beta$ Cooperates with the MYC Breast Cancer Oncogene

Transformation often results from cooperation among several oncogenes. We previously demonstrated that SRSF1 cooperates with MYC (Anczuków et al., 2012), one of the most frequently altered genes in cancer. It remains unknown whether this cooperation extends to other SR proteins. Here, we generated MCF-10A cells OE selected SFs together with an inducible MYC transgene (Eilers et al., 1989). TRA2 $\beta$ -OE together with MYC promoted the formation of enlarged acinar structures compared to either alone (Figures 4A and 4B). In contrast, no significant differences in size or morphology were observed following OE of SRSF6 or SRSF4 with MYC (Figure 4B). Further-

more, MYC and TRA2 $\beta$  are co-expressed at high levels in human breast tumors and in other tumor types (Figure 4C). In addition, TRA2 $\beta$  mRNA levels increased 4 h after MYC induction in MCF-10A cells (Figure 4D), which is consistent with the time frame for the transcriptional activation of known MYC targets (Das et al., 2012; Jung et al., 2008; Oran et al., 2016; Yap et al., 2011). Increased TRA2 $\beta$  protein levels are detected at 24 h (Figure 4D), suggesting that TRA2 $\beta$  is likely a direct transcriptional target of MYC. Direct binding of MYC to the TRA2 $\beta$  proximal promoter region is further supported by genome-wide chromatin immunoprecipitation (ChIP) sequencing (ChIP-seq) data from mammary MCF-7 and MCF-10A cells (Figure 4E). Finally, MYC is amplified and/or upregulated in 51% of TRA2 $\beta$ -high versus 26% of TRA2 $\beta$ -low breast tumors (Figure 4F). Thus, our findings suggest that TRA2 $\beta$ -OE may be driven by MYC alterations in at least a subset of breast tumors.

### Differential Role of SFs in Cell Migration and Invasion

To assess how SF-OE affects cell migration and invasion, we assayed several migratory or invasive phenotypes using 2D and 3D assays in non-invasive MCF-10A cells. In 3D collagen-Matrigel assays, the formation of intra-acinar bridges and multicellular protrusions, indicative of invasive behavior, was observed in 25%–50% of SRSF4-, TRA2 $\beta$ -, HNRNPA1-, and SRSF6-OE acini, but in <1% of control acini (Figures 5A and 5B). SRSF4-, TRA2 $\beta$ -, and SRSF6-OE also increased intra-acinar cell movement as detected by live-cell imaging (Figure S5A), and SRSF6-OE increased cell migration in 2D transwell assays (Figure S5C). Despite the lack of effect of SRSF9-OE on acinar morphology or size, SRSF9-OE cells migrated faster in wound-healing and transwell migration assays (Figures S5B and S5C) and exhibited invasive behavior in 3D assays (Figures 5A and 5B). These results suggest that SF-OE can affect cell invasion without affecting cell proliferation in MCF-10A cells.

To complement this analysis, which identified SFs that increase migratory properties in non-transformed MCF-10A cells, we asked whether SF levels are required to maintain migratory phenotypes in established breast cancer cells with metastatic potential (Figures 5C–5G). We focused on a TNBC model, as TRA2 $\beta$  is upregulated in 40% of TNBC tumors. We examined how SRSF4, SRSF6, SRSF9, and TRA2 $\beta$ , which increased migration and invasion in MCF-10A cells when overexpressed, affected the invasion of human MDA-MB231 TNBC cells. We established stable cell lines with a doxycycline (DOX)-inducible short hairpin RNA (shRNA) expression system that enables the tracking of retroviral transduction and shRNA induction through two fluorescent reporters—constitutively expressed GFP and DsRed expressed with the shRNA (Zuber et al., 2011). Six shRNAs were tested for each SF and the two shRNAs with the

### Figure 3. SF Overexpression Is Associated with Differentially Spliced Events in MCF-10A

- (A) DSEs detected by RNA-seq in SF-OE versus control MCF-10A day 8 acini (n = 3;  $|\Delta\text{PSI}| \geq 10\%$ , false discovery rate [FDR] < 5%, p < 0.01), sorted by AS event types. CA, cassette exon; MXE, mutually exclusive exon; RI, retained intron; A5'/SS, alternative 5' splice site; A3'/SS, alternative 3' splice site.  
 (B) Skipped ( $\Delta\text{PSI} \leq -10\%$ ) and included ( $\Delta\text{PSI} \geq 10\%$ ) DSEs in SF-OE versus control are plotted by  $\Delta\text{PSI}$  values for each SF for all AS event types.  
 (C) Overlap in DSEs for each SF pair. Bubble size is proportional to the number of shared DSEs and color indicates p values.  
 (D) RT-PCR validations of DSEs. A representative gel is shown, along with isoform structures. PSI for all samples and  $\Delta\text{PSI}$  for significant SFs are calculated from RT-PCR (n = 3; mean  $\pm$  SD; t test, \*p < 0.05, n.s., not significant) and RNA-seq.  
 See also Figure S4 and Table S3.

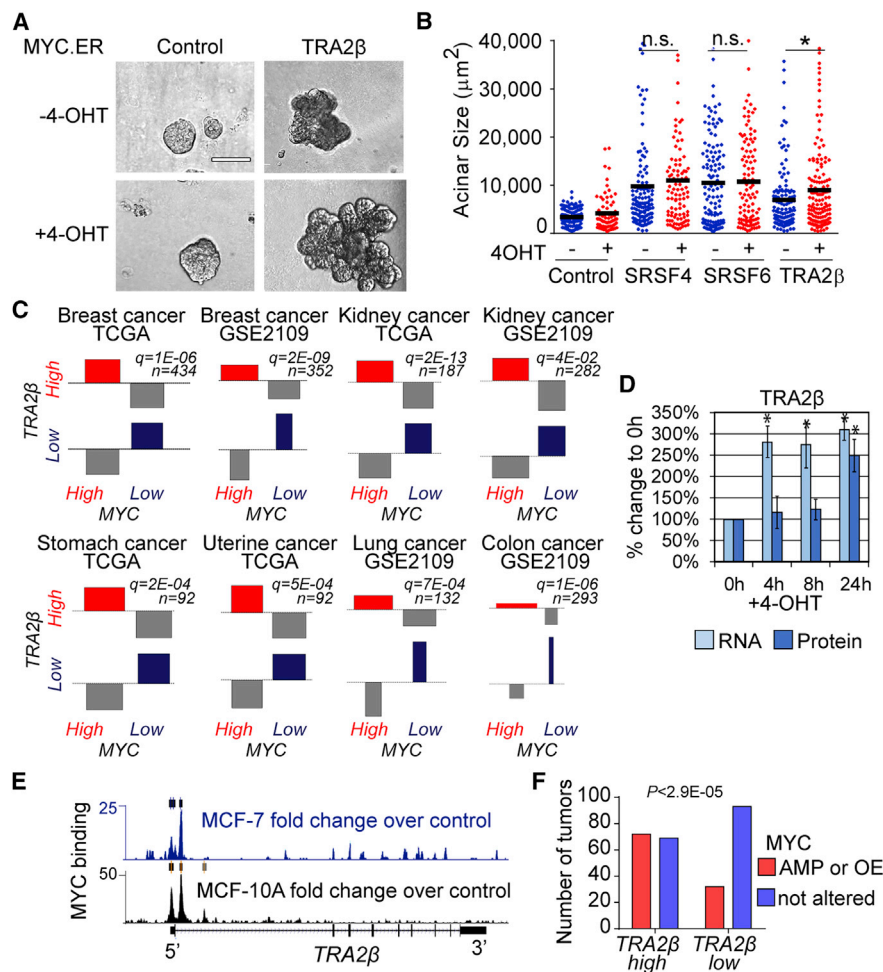


**Figure 4. Cooperation of TRA2β with the MYC Oncogene in Breast Cancer**

(A) Representative bright-field images of control or TRA2β-OE 3D MCF-10A acini expressing estrogen receptor ligand-binding domain (ER)-inducible MYC, activated by 4-hydroxytamoxifen (4-OHT) (scale bar: 100  $\mu\text{m}$ ).

(B) Acinar size distribution and median (horizontal line) of SRSF4-, SRSF6-, TRA2β-OE MYC.ER MCF-10A  $\pm$  4-OHT ( $n \geq 3$ , >100 acini per condition; t test, \* $p < 0.01$ , n.s., not significant).

(C) Association plot showing the correlation between MYC and TRA2β expression in human tumors. Dataset identification numbers (IDs) and numbers of samples are indicated. MYC and TRA2β expression are grouped into four categories: (1) both high, (2) TRA2β high and MYC low, (3) TRA2β low and MYC high, and (4) both low.

(D) The TRA2β RNA and protein levels in MYC.ER MCF-10A +4-OHT at indicated time points are measured by qRT-PCR and western blotting ( $n = 3$ ; mean  $\pm$  SD; t test, \* $p < 0.05$ ). RNA levels are normalized to GAPDH and HPRT; protein levels are normalized to tubulin.

(E) MYC binding to TRA2β genomic region as detected by MYC ChIP-seq experiments in MCF-7 and MCF-10A cells. Fold changes over control are calculated from pooled replicates; significant peaks are shown by rectangles.

(F) MYC amplification (AMP) or OE status in TRA2β-high versus TRA2β-low breast tumors.

strongest knockdown (KD) were used further (Figure 5C). SF-KD did not decrease cell-doubling time (Figures S5D and S5E), allowing us to define the effect of SF-KD on cell invasion independently of its potential effect on proliferation. TRA2β-KD decreased cell migration in wound healing and transwell migration assays (Figures 5D, 5E, S5F, and S5G). A milder phenotype was observed for SRSF4-KD, which decreased migration in wound healing assays only (Figure 5D). The relatively modest KD efficiency for SRSF6 and SRSF9 (Figure 5C) may limit our ability to detect their role in cell migration and invasion. However, we noted that despite modest KD, both SRSF9 shRNAs

decreased transwell migration to similar levels as TRA2β shRNAs (Figures 5E and S5G). SRSF9sh2+DOX cells, but not SRSF9sh1+DOX cells, migrated less in wound healing assays (Figure 5D), possibly because control SRSF9sh1-DOX cells migrated less on plastic than did SRSF9sh2-DOX cells (Figure S5F). Finally, we assessed SF-KD in MDA-MB231 cells grown in 3D culture in Matrigel, which form stellate structures representative of their invasive behavior. When shRNAs were induced from day 0, TRA2β-KD prevented the formation of stellate invasive structures and promoted the formation of round acinar-like structures lacking invasive behavior (Figures 5F and

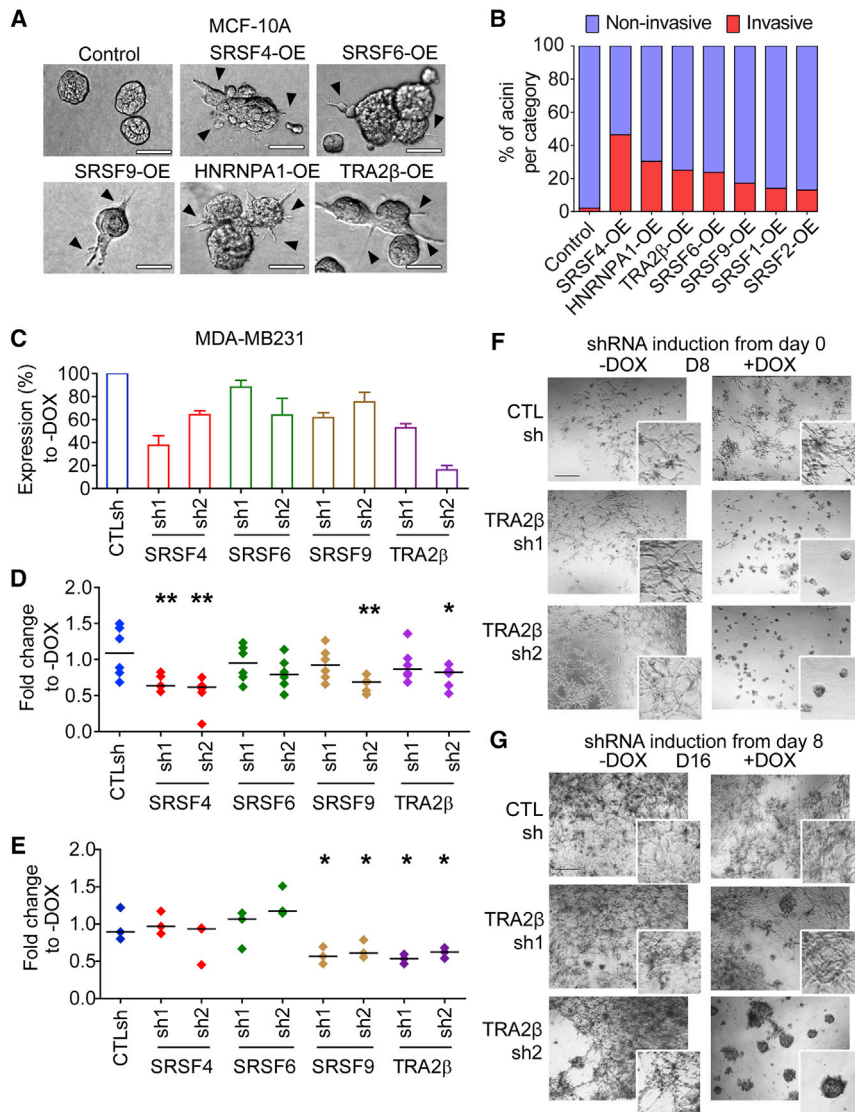


**Figure 5. Differential Roles of SFs in Cell Migration and Invasion**

(A) Representative bright-field images of acinar morphology for control or SF-OE 3D MCF-10A cells grown in Matrigel-collagen invasion assay at day 8. Multicellular protrusions and inter-acinar bridges are indicated by arrowheads (scale bar: 50  $\mu$ m).

(B) Percentage of invasive versus non-invasive acini at day 8 (n = 3, >50 acini per condition).

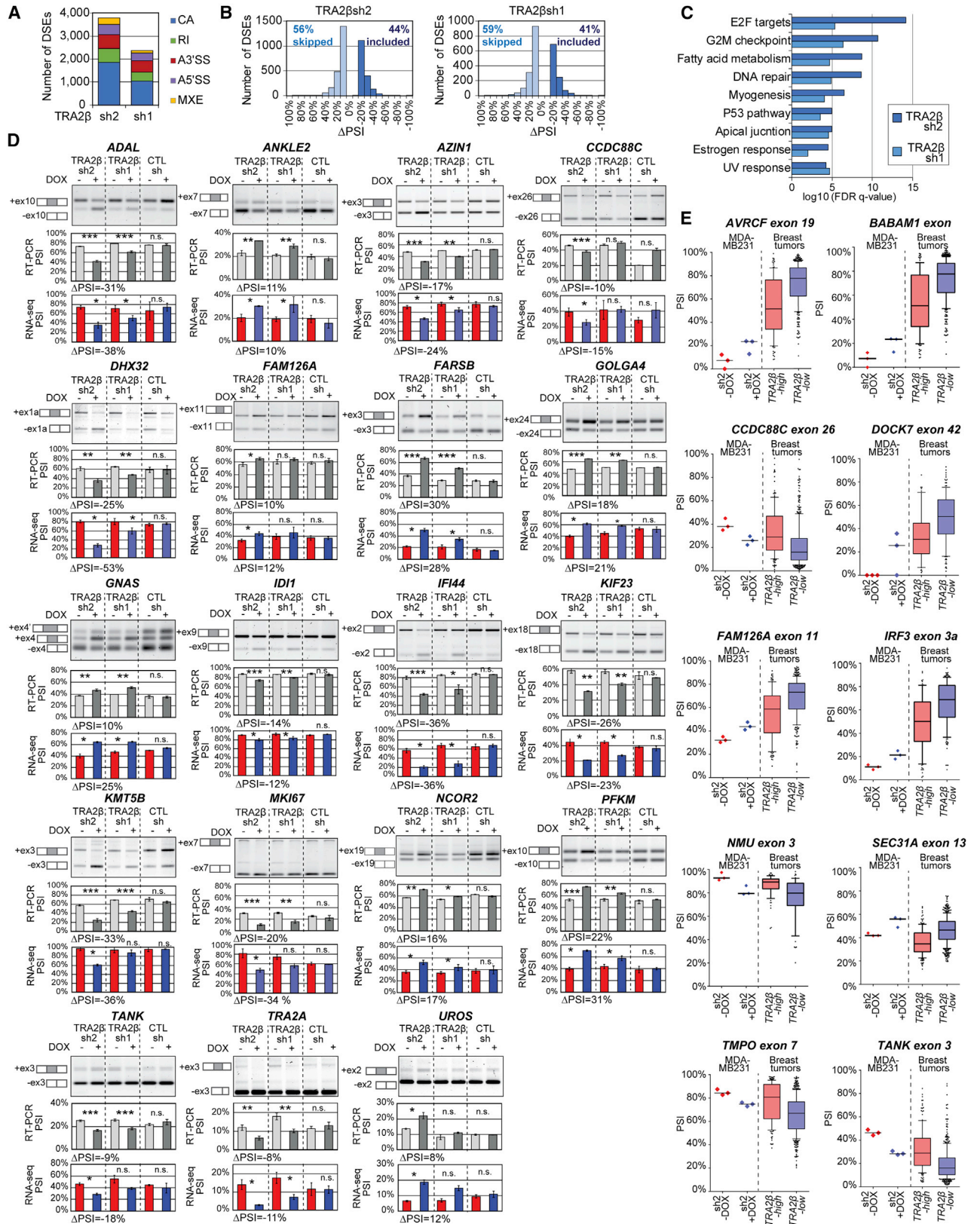
(C) SF levels in MDA-MB231 expressing scrambled CTLsh or SF-targeting shRNAs are quantified 72 h after DOX treatment by western blotting using SF-specific antibodies and normalized to tubulin. Percentage of SF in +DOX is normalized to the corresponding -DOX (n = 3; mean  $\pm$  SD).

(D and E) Migration of CTLsh or SFsh MDA-MB231  $\pm$  DOX in 2D wound-healing (D) or transwell assay (E). Distribution and median (horizontal line) for each condition +DOX normalized to -DOX (n = 3; t test, \*p < 0.05, \*\*p < 0.005).

(F and G) Representative bright-field images of CTLsh or TRA2 $\beta$ sh MDA-MB231 cells, grown in 3D  $\pm$  DOX (scale bar: 100  $\mu$ m). DOX is added from either day 0 (F) or day 8 (G). See also Figures S5 and S6.

S5H–S5J). SRSF6-KD also prevented the formation of invasive structures, whereas SRSF4- and SRSF9-KD decreased the number of stellate structures and their size (Figures S5H and S5I). Finally, using the inducible system, we tested whether TRA2 $\beta$  is required to maintain cell invasion. TRA2 $\beta$ -shRNA induction on day 8, after the formation of invasive structures, was sufficient to reverse the phenotype and promote the formation of non-invasive acinar-like structures (Figure 5G). The effect was dose dependent, as the weaker shRNA, TRA2 $\beta$ sh1, had an intermediate phenotype compared to TRA2 $\beta$ sh2 (Figure 5G). We further demonstrate that TRA2 $\beta$ -KD prevented the formation of stellate invasive structures in another TNBC cell line, SUM159PT (Figures S6A and S6B). In summary, our findings suggest that specific SFs play a role in controlling cell migration in MCF-10A cells or in maintaining the invasive potential of breast cancer cells. In particular, TRA2 $\beta$  expression was sufficient to initiate invasion in mammary MCF-10A cells and was required to maintain invasiveness in MDA-MB231 and SUM159PT cells.

from TRA2 $\beta$ sh+DOX versus -DOX were discarded if they were also significant and altered in the same direction in CTLsh+DOX versus -DOX (Table S5A). Following the exclusion of DOX-induced events, we identified >3,500 DSEs in TRA2 $\beta$ sh2+DOX, and >2,000 in TRA2 $\beta$ sh1+DOX (Figure 6A; Tables S5B and S5C); the number of DSEs associated with the stronger shRNA TRA2 $\beta$ sh2 was higher than the number associated with the weaker shRNA. TRA2 $\beta$ sh1+DOX and TRA2 $\beta$ sh2+DOX cells shared 582 DSEs and 691 DSGs (Tables S5E and S5F). TRA2 $\beta$ -KD promoted primarily CA events, favoring skipping over inclusion (Figures 6A and 6B). TRA2 $\beta$ -KD affected the AS of genes that regulate key cellular processes associated with transformation (Figure 6C). Analysis of breast cancer-associated genes with alternatively spliced protein domains revealed that TRA2 $\beta$ -regulated targets are enriched in genes associated with G2/M regulation, protein deubiquitination, DNA repair, cell migration, and apoptosis (Tables S5G and S5H). These biological processes were also highly ranked



(legend on next page)

in *TRA2 $\beta$*  targets in MCF-10A cells, albeit represented by a different set of genes (Table S5H). These observations presumably reflect differences in the isoforms that are associated with *TRA2 $\beta$*  function in mammary transformation in MCF-10A cells versus its role in tumor maintenance and invasion in MDA-MB231 cells.

We validated 16 *TRA2 $\beta$* -regulated DSEs by RT-PCR in 3D-grown MDA-MB231 cells (Figure 6D) out of 21 randomly selected DSEs. Validated DSEs affect genes associated with mitosis (*ADAL*), migration and adhesion (*DHX32*, *IFI44*, *KMT5B*, *KIF23*, *TANK*), signaling (*FAM126A*, *CCDC88C*, *GNAS*, *NCOR2*, *TANK*), AS (*TRA2 $\alpha$* ), or metabolism (*ADAL*, *FARSB*, *IDI1*, *UROS*, *PFKM*). Furthermore, we demonstrated that 5 out of 6 *TRA2 $\beta$* -regulated DSEs detected in MDA-MB231 cells are also differentially spliced in SUM159PT cells with *TRA2 $\beta$* -sh2 (Figures S6A–S6C).  $\Delta$ PSI magnitude is smaller in SUM159PT compared to MDA-MB231, which is consistent with a lower *TRA2 $\beta$* -KD efficiency in SUM159PT.

*TRA2 $\beta$* -KD also affected gene expression in 3D MDA-MB231 cells (Table S6), with >1,400 up- and >1,200 downregulated genes in *TRA2 $\beta$* sh2 (Table S6B), whereas the weaker hairpin had an intermediate effect (Table S6C). DEGs were associated with Wnt signaling, cell polarity, cell cycle, and transcriptional control (Table S6D). Differential AS also led to changes in gene expression, with 312 genes affected both at the AS and the gene expression levels (Table S6E).

To further uncover spliced isoforms that are relevant to human breast tumors, we focused on DSEs detected both in MDA-MB231 cells and breast tumors with high *TRA2 $\beta$*  levels. We identified 32 shared DSEs, defined as DSEs regulated in opposite directions—in other words,  $\Delta$ PSI  $\geq$  10% in *TRA2 $\beta$* sh2+DOX versus –DOX MDA-MB231 and  $\Delta$ PSI  $\leq$  –10% in *TRA2 $\beta$* -high versus *TRA2 $\beta$* -low tumors, and vice versa (Figure 6E; Table S5K). These DSEs affect genes associated with cell invasion and metastasis (*ARVCF*, *DOCK7*, *TANK*, *TMPO*, *CCDC88C*, *SEC31A*), cell cycle (*TMPO*), signaling (*FAM126A*, *IRF3*, *NMU*), or DNA replication and repair (*BABAM1*) (Table S5I). Finally, we assayed the function of two *TRA2 $\beta$* -regulated isoforms, *TANK*+ex3 and *CCDC88C*+ex26, both included at higher levels in MDA-MB231 and breast tumors with *TRA2 $\beta$* -high levels (Figures 6D–6F). Both *TANK* and *CCDC88C* genes were implicated in cell invasion (Ishida-Takagishi et al., 2012; Stelzig et al., 2013), although the function of these specific isoforms had yet to be characterized. MDA-MB231 cells expressing isoform-specific shRNAs targeting the *TANK*+ex3 isoform formed smaller and less invasive structures than control cells (*TANK*+ex3 sh +DOX versus –DOX), at least partially recapitulating the phenotype of *TRA2 $\beta$* -KD (Figures S6E–S6G). Isoform-specific KD of *CCDC88C*+ex26 had a weaker phenotype, with only sh2 leading

to smaller and less invasive structures (Figures S6F and S6G). Overall, our findings suggest that *TRA2 $\beta$*  regulates the AS of multiple genes linked with cancer and/or metastasis in both breast cancer cell lines and patients' tumor tissues.

### **TRA2 $\beta$ Plays a Role in Breast Cancer Metastasis *In Vivo*, and Its Expression Correlates with Clinical Outcomes in Breast Cancer Patients**

To assess the effect of *TRA2 $\beta$* -KD on metastasis *in vivo*, *TRA2 $\beta$* sh2 or CTLsh MDA-MB231 cells were orthotopically injected in the mammary gland of NOD.Cg-*Prkdc*<sup>scid</sup> *Il2rg*<sup>tm1Wjl</sup>/SzJ (NSG) female mice (Figure 7A). Primary tumor and metastasis formations were monitored by luciferin bioluminescence imaging and histology. *TRA2 $\beta$* -KD did not prevent the formation of primary mammary tumors (Figures 7B and S7A–S7C), nor did it affect their size, compared to non-induced (*TRA2 $\beta$* sh2+DOX versus –DOX) and induced controls (*TRA2 $\beta$* sh2+DOX versus CTLsh+DOX) (Figure S7B). However, *TRA2 $\beta$* -KD animals had a decrease in lung and liver metastatic burden compared to non-induced and induced controls (Figures 7C and 7D), and in lung, liver, or lymph node macro-metastases (Figure S7D). *TRA2 $\beta$* -KD reduced the number of metastatic foci, but had no effect on foci size (Figures S7B–S7J). In addition, *TRA2 $\beta$* -KD also reduced lung metastasis formation in an experimental metastasis model in which cancer cells are injected in the tail vein (Figures S7K–S7N), modeling the latter steps of the metastatic cascade (e.g., survival in circulation, extravasation, colonization of a distant site). Finally, clinical data for human breast tumors revealed that *TRA2 $\beta$* -high levels are associated with a decrease in overall survival (Figure 7E) and in distant metastasis-free survival (Figure 7F) in multiple patient cohorts. Overall, our data strongly suggest a role for *TRA2 $\beta$*  and its targets in the regulation of breast cancer metastasis initiation and maintenance.

## **DISCUSSION**

### **SF Alterations in Mammary Cells Have Distinct Functional Consequences**

Abnormal AS has emerged as a hallmark of human tumors (Urbanski et al., 2018). Defects in SFs are associated with many tumor types (Dvinge et al., 2016), yet the functional role of most SFs in tumorigenesis remains poorly characterized. Here, we identify alterations in the SR protein family and their frequency in human breast tumors. We then use breast cancer models to define the functional consequences of these SF alterations and identify their targets, uncovering distinct functions for each SR protein in mammary tissues. Our analysis of >900 human breast tumors revealed that SFs are frequently altered, but exhibit distinct alteration patterns and subtype specificity. In addition to

### **Figure 6. *TRA2 $\beta$* -KD Promotes Changes in Spliced Isoforms in 3D MDA-MB231 Cells**

(A) DSEs detected by RNA-seq in *TRA2 $\beta$* sh2 or *TRA2 $\beta$* sh1 MDA-MB231 cells, grown in 3D  $\pm$  DOX, at day 8 (n = 3;  $|\Delta$ PSI|  $\geq$  10%, FDR < 5%, p < 0.01).

(B) Skipped ( $\Delta$ PSI  $\leq$  –10%) and included ( $\Delta$ PSI  $\geq$  10%) DSEs in *TRA2 $\beta$* sh2 or *TRA2 $\beta$* sh1 +DOX versus –DOX plotted by  $\Delta$ PSI values.

(C) Gene set enrichment analysis for DSEs in *TRA2 $\beta$* sh2 or *TRA2 $\beta$* sh1 MDA-MB231 cells showing the top 10 hallmark gene sets.

(D) RT-PCR validations of selected DSEs. A representative gel is shown, along with isoform structures. PSI for all samples and  $\Delta$ PSI for *TRA2 $\beta$* sh2 are calculated from RT-PCR (n = 3; mean  $\pm$  SD; t test, \*p < 0.05, \*\*p < 0.005, \*\*\*p < 0.0005, n.s., not significant) and RNA-seq.

(E) PSI for DSEs detected both in *TRA2 $\beta$* -high versus *TRA2 $\beta$* -low breast tumors (n = 146 and 449) and MDA-MB231 cells.

See also Table S5.

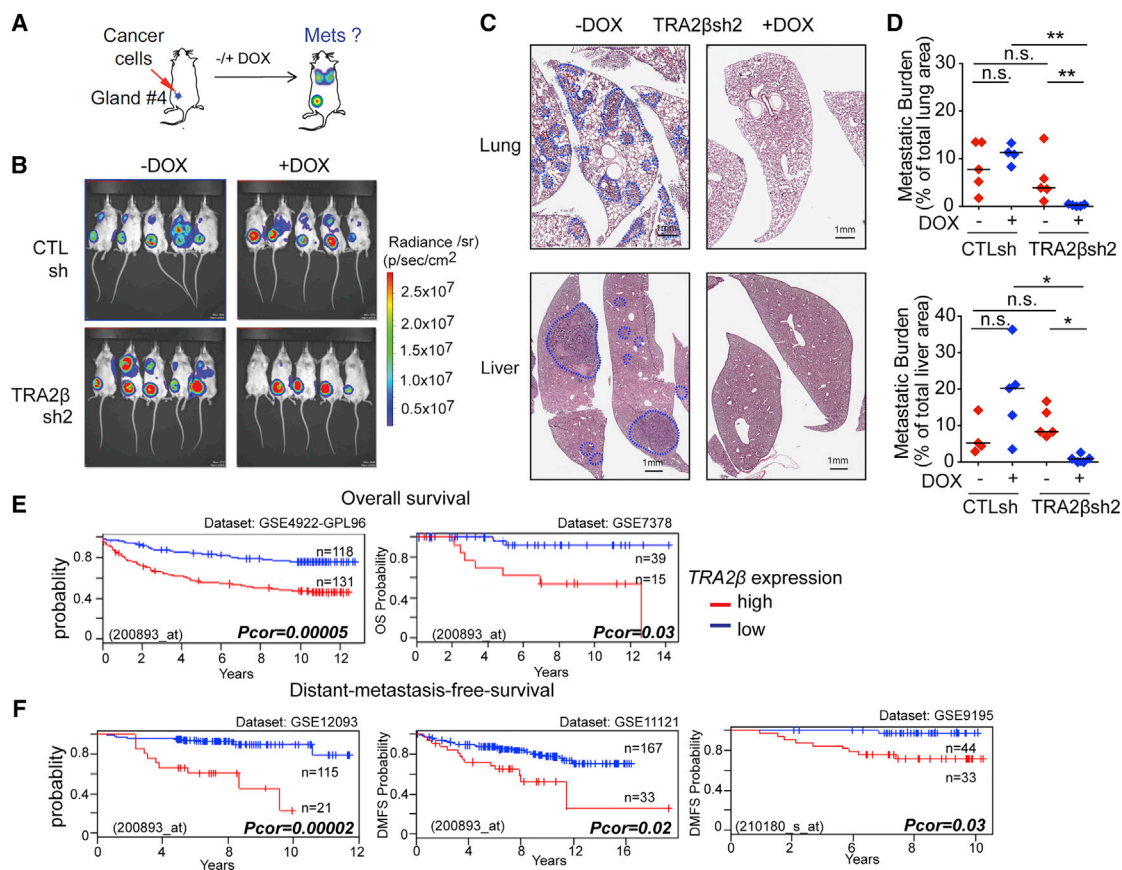


**Figure 7. TRA2 $\beta$  Plays a Role in Metastasis *In Vivo* in a TNBC Mouse Model and in Breast Cancer Patients**

(A) CTLsh or TRA2 $\beta$ sh2MDA-MB231 cells are injected into the mammary fat pad of NSG mice; primary tumors and metastasis are monitored by bioluminescence imaging.

(B) Bioluminescence detection of primary tumors and metastasis in mice injected with CTLsh or TRA2 $\beta$ sh2 MDA-MB231 cells  $\pm$  DOX at 8 weeks post-injection.

(C) Representative H&E lung and liver sections of mice injected with TRA2 $\beta$ sh2 MDA-MB231 cells  $\pm$  DOX (scale bar: 1 mm). Metastatic areas are circled in blue.

(D) Quantification of metastasis burden in mice injected with CTLsh or TRA2 $\beta$ sh2 MDA-MB231 cells  $\pm$  DOX ( $n \geq 4$ ; t test, \* $p < 0.01$ , \*\* $p < 0.001$ , n.s., not significant).

(E and F) Correlation between TRA2 $\beta$  expression and overall survival (E) or distant metastasis-free survival (F) in cohorts of breast cancer patients stratified by TRA2 $\beta$  levels. Cohort size, dataset, and probe ID, and corrected p value (log-rank test) are indicated.

See also Figure S7.

the breast cancer oncogene *SRSF1* (Anczuków et al., 2012), TRA2 $\beta$ , *SRSF2*, and *SRSF6* are each overexpressed in  $\geq 10\%$  of tumors, all subtypes combined. TRA2 $\beta$ -, *SRSF12*-, *SRSF3*-, and *SRSF2-high* tumors represent  $>20\%$ – $40\%$  of TNBCs, the most aggressive breast cancer subtype. Tumors with high levels of a given SF exhibit unique DSEs, and many DSEs are recurrently detected in  $>100$  tumors. In addition, tumors with alterations in distinct SFs share relatively low numbers of DSEs, with the exception of *SRSF3-high* and *SRSF7-high* tumors, which share 46% of their DSEs. Our findings thus suggest that distinct SFs have different targets and biological functions in breast tumors.

Not all SFs confer oncogenic properties in our model. Although *SRSF2* is upregulated in 13% of breast tumors, *SRSF2*-OE did not affect the phenotypes measured in MCF-10A cells. Recurrent mutations in *SRSF2* are found in human hematologic malignancies, but not in other tumor types (Urbanski et al., 2018). Functionally, blood lineage-specific expression of

*Srsf2*<sup>P95H</sup> causes defective hematopoiesis, and *SRSF2* mutations alter its binding preference, thereby altering its target recognition (Kim et al., 2015). Our findings demonstrate that changes in *SRSF2* levels trigger relatively few AS alterations in MCF-10A cells and that *SRSF2* may not contribute to the early steps of mammary transformation. Our study also suggests a restricted role for *SRSF9* in mammary tumorigenesis, which when overexpressed in MCF-10A cells increases cell migration and invasion, but does not affect cell proliferation, apoptosis, or acinar architecture. Consistently, *SRSF9* plays a role in cell invasion in bladder cancer (Yoshino et al., 2012), and *SRSF9*-OE promotes  $\beta$ -catenin accumulation and activates Wnt signaling (Fu et al., 2013), thus possibly linking *SRSF9* and cell invasion regulation. In summary, our findings reveal that *SRSF4*, *SRSF6*, and TRA2 $\beta$  play a role in both mammary transformation and metastasis, whereas *SRSF9* affects only cell invasion in the models tested. Thus, in mammary cells, distinct SFs may be

involved in each of the steps of tumorigenesis—some affecting cell proliferation, others invasion, and a subset promoting both, either directly or indirectly through downstream targets.

### The AS Repertoire of SR Proteins in Mammary Cells Provides a Functional Link to Their Role in Breast Cancer

Our analysis reveals that in MCF-10A cells, SRSF4, SRSF6, and TRA2 $\beta$  regulate not only shared AS isoforms but also a set of shared genes associated with biological processes involved in transformation and metastasis. Several SF-induced AS isoforms detected in this study (*ARHGEF11*, *RALGPS2*, *MLPH*, *CD44*, and *APLP2*) were previously associated with the epithelial-mesenchymal transition (EMT) (Brown et al., 2011; Harvey et al., 2018; Shapiro et al., 2011; Warzecha et al., 2010), which is consistent with the invasive phenotype of SF-OE MCF-10A cells. In addition, several validated DSEs have been linked with cell invasion or proliferation: (1) *ARHGEF11+ex38* is found in invasive basal breast cancer cells, but not in non-invasive luminal cells, and is required for cell migration and growth *in vitro* and *in vivo* (Itoh et al., 2017). The *ARHGEF11+ex38* isoform is unable to interact with tight-junction protein ZO-1 and is localized away from cell-cell junctions (Itoh et al., 2017). (2) The AS switch from *CD44v* to *CD44s* isoforms is associated with tumor progression (Chen et al., 2018), and *CD44s* isoforms can potentiate Akt activation and promote cell survival (Brown et al., 2011). (3) Lipolysis-stimulated lipoprotein receptor (LSR) expression is linked with breast cancer cell migration, and differences in its cellular localization are associated with patient outcomes (Reaves et al., 2017). Skipping of exon 5, encoding the transmembrane domain, could affect LSR localization and activity. (4) *TCF7L2* encodes a protein that interacts with  $\beta$ -catenin and plays a role in Wnt signaling. The *TCF7L2+ex4* isoform displays a reduced ability to activate Wnt/ $\beta$ -catenin targets (Weise et al., 2010). (5) The *MKI67 $\Delta$ ex7* isoform lacks 360 amino acids compared to the full-length protein, and is associated with nutrient-starvation response (Chierico et al., 2017).

A subset of SR proteins can shuttle between the nucleus and the cytoplasm, including SRSF1, SRSF3, SRSF4, SRSF6, SRSF7, and SRSF10 (Cáceres et al., 1998; Cazalla et al., 2002; Sapra et al., 2009), and this ability may depend on the differentiation state of the cell (Botti et al., 2017). Moreover, several SR proteins have splicing-independent functions—for example, SRSF1, SRSF3, and SRSF7 regulate mRNA export (Huang et al., 2004; Müller-McNicoll et al., 2016); SRSF1 and SRSF2 are implicated in nonsense-mediated mRNA decay (Aznarez et al., 2018; Sato et al., 2008; Zhang and Krainer, 2004); SRSF1 regulates translation by interacting with components of the mammalian target of rapamycin (mTOR) pathway (Maslon et al., 2014; Michlewski et al., 2008; Sanford et al., 2004, 2008); and SRSF3, SRSF5, SRSF6, and SRSF7 affect the translation of viral RNA (Bedard et al., 2007; Fitzgerald and Semler, 2011, 2013; Swanson et al., 2010; Swartz et al., 2007). In the present study, we cannot exclude the possibility that the described SF-associated phenotypes result from a dual role of the SF in AS and in mRNA export or translation, or other as yet to be defined functions. Potential non-splicing-related functions of SRSF4, SRSF6, and TRA2 $\beta$  in human cells warrant further investigation.

### TRA2 $\beta$ Controls Mammary Cell Transformation and Breast Tumor Metastasis

TRA2 $\beta$  is overexpressed in many tumor types, and a role in tumorigenesis has been proposed (Best et al., 2013). Here, we provide a characterization of the function of TRA2 $\beta$  in promoting mammary cell transformation and metastasis *in vitro* and *in vivo*. TRA2 $\beta$ -OE tumors represent >40% of TNBCs, an aggressive breast cancer subtype with high metastasis incidence. Our results suggest that modulating TRA2 $\beta$  levels may represent a viable therapeutic option, even for patients with advanced metastatic disease.

In MDA-MB231 cells, TRA2 $\beta$  controls the AS of target genes associated with cell invasion, Wnt signaling, cell polarity, cell cycle, and transcriptional control. For example, high TRA2 $\beta$  levels in both TNBC cells and human tumors are associated with the AS of *TANK*, a member of the tumor necrosis factor receptor-associated factor protein family, which has been linked with cell proliferation and migration in brain tumors (Stellzig et al., 2013). The inclusion of *TANK* exon 3 encodes 58 additional amino acids in the N-terminal domain, which could affect the function of the protein. Using isoform-specific KD, we demonstrate that the exon 3-containing isoform is important for cell invasion in MDA-MB231 cells. Another TRA2 $\beta$ -regulated target, *CCDC88C*, encodes a signal transducer and Wnt signaling regulator, which can trigger cell invasion and drive metastasis (Ishida-Takagishi et al., 2012). *CCDC88C* has multiple spliced isoforms that differ in their ability to enhance cell invasiveness (Ear et al., 2019). The isoform detected here includes exon 26, which introduces a premature termination codon (PTC), truncating 493 amino acids and producing a transcript that could be degraded by nonsense-mediated mRNA decay (NMD). In addition, TRA2 $\beta$ -KD alters the AS of *KMT5B*, encoding the lysine methyltransferase SUV420H1, which targets histone H4. Reduced H4K20me3 levels are detected in breast tumors, and SUV420H1-OE can suppress cell invasion (Yokoyama et al., 2014). TRA2 $\beta$  also regulates the AS of *KIF23*, which encodes a kinesin-like protein involved in microtubule formation and movement. High *KIF23* expression is associated with decreased overall survival and distant metastasis-free survival in breast cancer patients, and *KIF23*-KD suppresses the proliferation of TNBC cells (Wolter et al., 2017). Inclusion of exon 18 alters *KIF23* cellular localization and is associated with longer survival in liver cancer patients (Sun et al., 2015). Other TRA2 $\beta$  targets associated with cell invasion include *DOCK7*, a gene regulating Rac activation and ErbB2 signaling (Yamauchi et al., 2008), and *DPHS*, which activates RhoA signaling, leading to increased cell motility and invasion *in vitro* and increased tumor growth *in vivo* (Muramatsu et al., 2016). In addition, several TRA2 $\beta$ -regulated targets are associated with metabolism and cell signaling: inclusion of *FAM126A* exon 11 leads to a C-terminally truncated protein that could have distinct biological functions and affect phosphatidylinositol 4-kinase (PI4K) localization (Baskin et al., 2016). PI4K is frequently amplified in breast tumors, and its expression promotes multi-acinar formation in MCF-10A cells (Pinke and Lee, 2011); AS of *GNAS* exon 3 regulates the expression of long and short *GNAS* isoforms, which display differences in localization and activities (Bastepe, 2007). *GNAS* amplification is found with breast cancer, and the expression of the long isoform leads

to enhanced cyclic AMP (cAMP) signaling (Garcia-Murillas et al., 2014). The specific functions of each of the TRA2 $\beta$ -regulated isoforms remain to be determined. One may hypothesize that each TRA2 $\beta$ -regulated isoform contributes to a distinct aspect of TRA2 $\beta$ -mediated transformation, similarly to SRSF1 targets in breast cancer (Anczuków et al., 2015), and that SF-mediated transformation results from activating an oncogenic AS program, in the same way that a transcription factor activates hundreds of transcriptional targets.

The molecular mechanisms through which TRA2 $\beta$  levels are altered in tumors remain poorly understood. TRA2 $\beta$  is upregulated in 13% of breast tumors, but only 11% of these tumors show amplification at the gene locus. Our findings suggest that TRA2 $\beta$  is a direct transcriptional target of the MYC oncogene, that both genes are frequently co-expressed in breast tumors, and that their co-expression increases mammary acinar size. Furthermore, we demonstrate that 51% of TRA2 $\beta$ -high breast tumors exhibited MYC amplification or upregulation, suggesting that MYC transcriptional activation accounts for at least half of the TRA2 $\beta$  alterations. These findings, together with previous studies (Das et al., 2012; David et al., 2010; Hsu et al., 2015; Koh et al., 2015), show that MYC plays a critical role in regulating the expression of several SFs linked to tumorigenesis and provides a rationale for targeting AS in MYC-driven tumors.

### RBPs as Breast Cancer Drivers

This study focused on the SR protein family and several related SFs. However, alterations in other SFs are reported in breast tumors and could contribute to transformation. In breast cancer, SF mutations remain rare; mutations in SF3B1 are detected in only 1.6% of breast tumors, all subtypes combined, whereas they are found in 20% of uveal melanomas and 70%–80% of myelodysplastic syndromes (Urbanski et al., 2018). Moreover, SF3B1 mutations are associated with luminal tumors, a breast cancer subtype that has a better prognosis than TNBC. Similarly, U2AF1, SRSF2, RBM10, QKI, and FUBP1 mutations are each found in <0.5% of TCGA breast tumors (Urbanski et al., 2018). Thus, in breast cancer, SF mutations may not represent the most valuable markers for tumor progression or therapeutics targets. Conversely, changes in SF levels are frequently detected and likely play a role in tumorigenesis. Beyond SR proteins, other SFs are dysregulated in breast tumors; hnRNPK, hnRNPM, PTBP1, and RBM10 are upregulated and RBM5 is both upregulated and downregulated (Urbanski et al., 2018). hnRNPM regulates the EMT in epithelial cells, in part by promoting the AS of CD44s and altering transforming growth factor  $\beta$  (TGF- $\beta$ ) signaling (Xu et al., 2014). PTBP1-OE increases cell proliferation, anchorage-independent growth, and invasion (He et al., 2014; Wang et al., 2008), whereas PTBP1-KD has the opposite effect (Wang et al., 2018). Furthermore, spliceosome inhibition with shRNAs or small molecules inhibits the growth of TNBC cells and patient-derived xenografts (Chan et al., 2017). Whether SF alterations trigger changes in shared DSEs or affect genes converging on pathways that lead to transformation remains to be determined. In addition, it is not yet known which SF alterations are drivers of tumor initiation and which result from a hyper-proliferative cell state. Our study reveals that specific SF

alterations can contribute to mammary transformation and/or metastasis and also identifies two SFs upregulated in breast tumors but not sufficient by themselves to promote transformation in the models tested. These findings suggest that not all SF alterations are oncogenic in the mammary context or that they may require additional hits to cooperate in transformation. Given that tumors often exhibit alterations in multiple SFs, future studies should aim to understand how individual SFs regulate one another and whether they cooperate in transformation.

### STAR★METHODS

Detailed methods are provided in the online version of this paper and include the following:

- KEY RESOURCES TABLE
- LEAD CONTACT AND MATERIALS AVAILABILITY
- EXPERIMENTAL MODEL AND SUBJECT DETAILS
  - Human Cell Lines
  - Mice
- METHOD DETAILS
  - Plasmids
  - Cell Culture and Cell Lines
  - Three-Dimensional Morphogenesis Assay
  - Immunofluorescence
  - Quantitative RT-PCR Analysis
  - Western Blot Analysis
  - RNA-Sequencing Library Preparation
  - RT-PCR Splicing Event Validation
  - Wound-Healing Assays
  - Transwell Migration Assays
  - 3D Invasion Assays
  - MTT Assay
  - *In Vivo* Metastasis Modeling
  - Differential Splicing Analysis
  - TCGA Data Analysis
  - Differential Splicing Analysis of MCF-10A and MDA-MB231 Cell Lines
  - Pairwise Comparison of DSEs Across Multiple Studies
  - Differential Gene Expression Analysis
  - Protein Domain Annotation
  - Annotation of Genes with Breast Cancer Relevance
  - Gene Enrichment Analysis
  - MYC and TRA2 $\beta$  Association Analysis
  - MYC Binding Data
  - TRA2 $\beta$  Expression and Clinical Outcome Analysis
  - Graphs and Figures
- QUANTIFICATION AND STATISTICAL ANALYSIS
- DATA AND CODE AVAILABILITY

### SUPPLEMENTAL INFORMATION

Supplemental Information can be found online at <https://doi.org/10.1016/j.celrep.2019.10.110>.

### ACKNOWLEDGMENTS

We thank J.E. Wilkinson for assistance with histopathology, S. Sampson and T. Helenius for comments on the manuscript, and M. Yurieva for assistance

with GEO submission. We acknowledge assistance from The Jackson Laboratory (JAX) and Cold Spring Harbor Laboratory (CSHL) Microscopy and Sequencing Shared Resources, funded by the National Cancer Institute (NCI) Cancer Center Support grants P30CA034196 and P30CA045508. This work was supported by grants from the NCI R00CA1728206 to O.A. and P01CA13106 to A.R.K.; National Institute of General Medical Sciences (NIGMS) R43GM116478 to M.A.; and postdoctoral awards to O.A. from the Susan G. Komen Foundation for the Cure (KG091029), the Terri Brodeur Breast Cancer Foundation (66810101), and JAX start-up funds. We acknowledge the use of data generated by TCGA, managed by NCI and the National Human Genome Research Institute (NHGRI), and processed using the Institute for Systems Biology (ISB) Cancer Genomics Cloud. The content is solely the responsibility of the authors and does not necessarily represent NIH official views.

### AUTHOR CONTRIBUTIONS

O.A. designed and supervised the study, conducted the experiments, analyzed the data, and wrote the paper. S.D. contributed to the *in vitro* and *in vivo* assays; S.D., S.H.P., M.B., L.U., N.L., L.H., and M.F. contributed to the *in vitro* assays; M.A. contributed to the bioinformatics tools development, analyses, and data interpretation; and A.G., A.K.K., J.G., I.H., and K.-T.L. contributed to bioinformatics. S.K.M. shared protocols and reagents. A.R.K. contributed to the study design and writing the paper. All of the authors discussed the results and the manuscript.

### DECLARATION OF INTERESTS

M.A. is a founder and shareholder of Envisagenics, Inc., and A.R.K. is a member of its scientific advisory board.

Received: July 3, 2019

Revised: September 9, 2019

Accepted: October 28, 2019

Published: November 26, 2019

### REFERENCES

Anczuków, O., Rosenberg, A.Z., Akerman, M., Das, S., Zhan, L., Karni, R., Muthuswamy, S.K., and Krainer, A.R. (2012). The splicing factor SRSF1 regulates apoptosis and proliferation to promote mammary epithelial cell transformation. *Nat. Struct. Mol. Biol.* *19*, 220–228.

Anczuków, O., Akerman, M., Cléry, A., Wu, J., Shen, C., Shirole, N.H., Raimer, A., Sun, S., Jensen, M.A., Hua, Y., et al. (2015). SRSF1-Regulated Alternative Splicing in Breast Cancer. *Mol. Cell* *60*, 105–117.

Aznarez, I., Nomakuchi, T.T., Tetenbaum-Novatt, J., Rahman, M.A., Fregoso, O., Rees, H., and Krainer, A.R. (2018). Mechanism of Nonsense-Mediated mRNA Decay Stimulation by Splicing Factor SRSF1. *Cell Rep.* *23*, 2186–2198.

Baskin, J.M., Wu, X., Christiano, R., Oh, M.S., Schauder, C.M., Gazzero, E., Messa, M., Baldassari, S., Assereto, S., Biancheri, R., et al. (2016). The leukodystrophy protein FAM126A (hyccin) regulates PtdIns(4)P synthesis at the plasma membrane. *Nat. Cell Biol.* *18*, 132–138.

Bastepe, M. (2007). The GNAS Locus: Quintessential Complex Gene Encoding G $\alpha$ alpha, X $\alpha$ alphas, and other Imprinted Transcripts. *Curr. Genomics* *8*, 398–414.

Bedard, K.M., Daijogo, S., and Semler, B.L. (2007). A nucleo-cytoplasmic SR protein functions in viral IRES-mediated translation initiation. *EMBO J.* *26*, 459–467.

Best, A., Dagliesh, C., Ehrmann, I., Kheirollahi-Kouhestani, M., Tyson-Capper, A., and Elliott, D.J. (2013). Expression of Tra2  $\beta$  in Cancer Cells as a Potential Contributory Factor to Neoplasia and Metastasis. *Int. J. Cell Biol.* *2013*, 843781.

Black, D.L. (2003). Mechanisms of alternative pre-messenger RNA splicing. *Annu. Rev. Biochem.* *72*, 291–336.

Bolger, A.M., Lohse, M., and Usadel, B. (2014). Trimmomatic: a flexible trimmer for Illumina sequence data. *Bioinformatics* *30*, 2114–2120.

Botti, V., McNicoll, F., Steiner, M.C., Richter, F.M., Solovyeva, A., Wegener, M., Schwich, O.D., Poser, I., Zarnack, K., Wittig, I., et al. (2017). Cellular differentiation state modulates the mRNA export activity of SR proteins. *J. Cell Biol.* *216*, 1993–2009.

Bradley, T., Cook, M.E., and Blanchette, M. (2015). SR proteins control a complex network of RNA-processing events. *RNA* *21*, 75–92.

Brown, R.L., Reinke, L.M., Damerow, M.S., Perez, D., Chodosh, L.A., Yang, J., and Cheng, C. (2011). CD44 splice isoform switching in human and mouse epithelium is essential for epithelial-mesenchymal transition and breast cancer progression. *J. Clin. Invest.* *121*, 1064–1074.

Cáceres, J.F., Misteli, T., Sreaton, G.R., Spector, D.L., and Krainer, A.R. (1997). Role of the modular domains of SR proteins in subnuclear localization and alternative splicing specificity. *J. Cell Biol.* *138*, 225–238.

Cáceres, J.F., Sreaton, G.R., and Krainer, A.R. (1998). A specific subset of SR proteins shuttles continuously between the nucleus and the cytoplasm. *Genes Dev.* *12*, 55–66.

Carvalho-Silva, D., Pierleoni, A., Pignatelli, M., Ong, C., Fumis, L., Karamanis, N., Carmona, M., Faulconbridge, A., Hercules, A., McAuley, E., et al. (2019). Open Targets Platform: new developments and updates two years on. *Nucleic Acids Res.* *47* (D1), D1056–D1065.

Cazalla, D., Zhu, J., Manche, L., Huber, E., Krainer, A.R., and Cáceres, J.F. (2002). Nuclear export and retention signals in the RS domain of SR proteins. *Mol. Cell. Biol.* *22*, 6871–6882.

Cerami, E., Gao, J., Dogrusoz, U., Gross, B.E., Sumer, S.O., Aksoy, B.A., Jacobsen, A., Byrne, C.J., Heuer, M.L., Larsson, E., et al. (2012). The cBio cancer genomics portal: an open platform for exploring multidimensional cancer genomics data. *Cancer Discov.* *2*, 401–404.

Chan, S., Sridhar, P., Kirchner, R., Lock, Y.J., Herbert, Z., Buonamici, S., Smith, P., Lieberman, J., and Petrocca, F. (2017). Basal-A Triple-Negative Breast Cancer Cells Selectively Rely on RNA Splicing for Survival. *Mol. Cancer Ther.* *16*, 2849–2861.

Chen, E.Y., Tan, C.M., Kou, Y., Duan, Q., Wang, Z., Meirelles, G.V., Clark, N.R., and Ma'ayan, A. (2013). Enrichr: interactive and collaborative HTML5 gene list enrichment analysis tool. *BMC Bioinformatics* *14*, 128.

Chen, C., Zhao, S., Karnad, A., and Freeman, J.W. (2018). The biology and role of CD44 in cancer progression: therapeutic implications. *J. Hematol. Oncol.* *11*, 64.

Chierico, L., Rizzello, L., Guan, L., Joseph, A.S., Lewis, A., and Battaglia, G. (2017). The role of the two splice variants and extranuclear pathway on Ki-67 regulation in non-cancer and cancer cells. *PLoS One* *12*, e0171815.

Climente-González, H., Porta-Pardo, E., Godzik, A., and Eyras, E. (2017). The Functional Impact of Alternative Splicing in Cancer. *Cell Rep.* *20*, 2215–2226.

Das, S., Anczuków, O., Akerman, M., and Krainer, A.R. (2012). Oncogenic splicing factor SRSF1 is a critical transcriptional target of MYC. *Cell Rep.* *1*, 110–117.

David, C.J., Chen, M., Assanah, M., Canoll, P., and Manley, J.L. (2010). HnRNP proteins controlled by c-Myc deregulate pyruvate kinase mRNA splicing in cancer. *Nature* *463*, 364–368.

Debnath, J., and Brugge, J.S. (2005). Modelling glandular epithelial cancers in three-dimensional cultures. *Nat. Rev. Cancer* *5*, 675–688.

Debnath, J., Mills, K.R., Collins, N.L., Reginato, M.J., Muthuswamy, S.K., and Brugge, J.S. (2002). The role of apoptosis in creating and maintaining luminal space within normal and oncogene-expressing mammary acini. *Cell* *111*, 29–40.

Debnath, J., Muthuswamy, S.K., and Brugge, J.S. (2003a). Morphogenesis and oncogenesis of MCF-10A mammary epithelial acini grown in three-dimensional basement membrane cultures. *Methods* *30*, 256–268.

Debnath, J., Walker, S.J., and Brugge, J.S. (2003b). Akt activation disrupts mammary acinar architecture and enhances proliferation in an mTOR-dependent manner. *J. Cell Biol.* *163*, 315–326.

- Dobin, A., Davis, C.A., Schlesinger, F., Drenkow, J., Zaleski, C., Jha, S., Batut, P., Chaisson, M., and Gingeras, T.R. (2013). STAR: ultrafast universal RNA-seq aligner. *Bioinformatics* 29, 15–21.
- Dvinge, H., Kim, E., Abdel-Wahab, O., and Bradley, R.K. (2016). RNA splicing factors as oncoproteins and tumour suppressors. *Nat. Rev. Cancer* 16, 413–430.
- Ear, J., Dunkel, Y., Mittal, M., Lim, B.B.C., Liu, L., Holda, M., Nitsche, U., Barbazan, J., Goel, A., Janssen, K.P., et al. (2019). Two Isoforms of the Guanine Nucleotide Exchange Factor, Daple/CCDC88C Cooperate as Tumor Suppressors. *Sci. Rep.* 9, 12124.
- Eilers, M., Picard, D., Yamamoto, K.R., and Bishop, J.M. (1989). Chimaeras of myc oncoprotein and steroid receptors cause hormone-dependent transformation of cells. *Nature* 340, 66–68.
- Eswaran, J., Horvath, A., Godbole, S., Reddy, S.D., Mudvari, P., Ohshiro, K., Cyanam, D., Nair, S., Fuqua, S.A., Polyak, K., et al. (2013). RNA sequencing of cancer reveals novel splicing alterations. *Sci. Rep.* 3, 1689.
- Fitzgerald, K.D., and Semler, B.L. (2011). Re-localization of cellular protein SRp20 during poliovirus infection: bridging a viral IRES to the host cell translation apparatus. *PLoS Pathog.* 7, e1002127.
- Fitzgerald, K.D., and Semler, B.L. (2013). Poliovirus infection induces the colocalization of cellular protein SRp20 with TIA-1, a cytoplasmic stress granule protein. *Virus Res.* 176, 223–231.
- Fu, Y., Huang, B., Shi, Z., Han, J., Wang, Y., Huangfu, J., and Wu, W. (2013). SRSF1 and SRSF9 RNA binding proteins promote Wnt signalling-mediated tumorigenesis by enhancing  $\beta$ -catenin biosynthesis. *EMBO Mol. Med.* 5, 737–750.
- Gao, J., Aksoy, B.A., Dogrusoz, U., Dresdner, G., Gross, B., Sumer, S.O., Sun, Y., Jacobsen, A., Sinha, R., Larsson, E., et al. (2013). Integrative analysis of complex cancer genomics and clinical profiles using the cBioPortal. *Sci. Signal.* 6, pl1.
- Garcia-Murillas, I., Sharpe, R., Pearson, A., Campbell, J., Natrajan, R., Ashworth, A., and Turner, N.C. (2014). An siRNA screen identifies the GNAS locus as a driver in 20q amplified breast cancer. *Oncogene* 33, 2478–2486.
- Ge, H., and Manley, J.L. (1990). A protein factor, ASF, controls cell-specific alternative splicing of SV40 early pre-mRNA in vitro. *Cell* 62, 25–34.
- Harvey, S.E., Xu, Y., Lin, X., Gao, X.D., Qiu, Y., Ahn, J., Xiao, X., and Cheng, C. (2018). Coregulation of alternative splicing by hnRNPM and ESRP1 during EMT. *RNA* 24, 1326–1338.
- He, X., Arslan, A.D., Ho, T.T., Yuan, C., Stampfer, M.R., and Beck, W.T. (2014). Involvement of polypyrimidine tract-binding protein (PTBP1) in maintaining breast cancer cell growth and malignant properties. *Oncogenesis* 3, e84.
- Hsu, T.Y., Simon, L.M., Neill, N.J., Marcotte, R., Sayad, A., Bland, C.S., Echeverria, G.V., Sun, T., Kurlay, S.J., Tyagi, S., et al. (2015). The spliceosome is a therapeutic vulnerability in MYC-driven cancer. *Nature* 525, 384–388.
- Huang, Y., Yario, T.A., and Steitz, J.A. (2004). A molecular link between SR protein dephosphorylation and mRNA export. *Proc. Natl. Acad. Sci. USA* 101, 9666–9670.
- Huang, C.S., Shen, C.Y., Wang, H.W., Wu, P.E., and Cheng, C.W. (2007). Increased expression of SRp40 affecting CD44 splicing is associated with the clinical outcome of lymph node metastasis in human breast cancer. *Clin. Chim. Acta* 384, 69–74.
- Huelga, S.C., Vu, A.Q., Arnold, J.D., Liang, T.Y., Liu, P.P., Yan, B.Y., Donohue, J.P., Shiue, L., Hoon, S., Brenner, S., et al. (2012). Integrative genome-wide analysis reveals cooperative regulation of alternative splicing by hnRNP proteins. *Cell Rep.* 1, 167–178.
- Ishida-Takagishi, M., Enomoto, A., Asai, N., Ushida, K., Watanabe, T., Hashimoto, T., Kato, T., Weng, L., Matsumoto, S., Asai, M., et al. (2012). The Dishevelled-associating protein Daple controls the non-canonical Wnt/Rac pathway and cell motility. *Nat. Commun.* 3, 859.
- Itoh, M., Radisky, D.C., Hashiguchi, M., and Sugimoto, H. (2017). The exon 38-containing ARHGEF11 splice isoform is differentially expressed and is required for migration and growth in invasive breast cancer cells. *Oncotarget* 8, 92157–92170.
- Jia, R., Li, C., McCoy, J.P., Deng, C.X., and Zheng, Z.M. (2010). SRp20 is a proto-oncogene critical for cell proliferation and tumor induction and maintenance. *Int. J. Biol. Sci.* 6, 806–826.
- Jung, P., Messen, A., Mayr, D., and Hermeking, H. (2008). AP4 encodes a c-MYC-inducible repressor of p21. *Proc. Natl. Acad. Sci. USA* 105, 15046–15051.
- Karni, R., de Stanchina, E., Lowe, S.W., Sinha, R., Mu, D., and Krainer, A.R. (2007). The gene encoding the splicing factor SF2/ASF is a proto-oncogene. *Nat. Struct. Mol. Biol.* 14, 185–193.
- Kim, E., Ilagan, J.O., Liang, Y., Daubner, G.M., Lee, S.C., Ramakrishnan, A., Li, Y., Chung, Y.R., Micol, J.B., Murphy, M.E., et al. (2015). SRSF2 Mutations Contribute to Myelodysplasia by Mutant-Specific Effects on Exon Recognition. *Cancer Cell* 27, 617–630.
- Koh, C.M., Bezzi, M., Low, D.H., Ang, W.X., Teo, S.X., Gay, F.P., Al-Haddawi, M., Tan, S.Y., Osato, M., Sabo, A., et al. (2015). MYC regulates the core pre-mRNA splicing machinery as an essential step in lymphomagenesis. *Nature* 523, 96–100.
- Krainer, A.R., Conway, G.C., and Kozak, D. (1990). Purification and characterization of pre-mRNA splicing factor SF2 from HeLa cells. *Genes Dev.* 4, 1158–1171.
- Kuleshov, M.V., Jones, M.R., Rouillard, A.D., Fernandez, N.F., Duan, Q., Wang, Z., Koplev, S., Jenkins, S.L., Jagodnik, K.M., Lachmann, A., et al. (2016). Enrichr: a comprehensive gene set enrichment analysis web server 2016 update. *Nucleic Acids Res.* 44 (W1), W90–W97.
- Long, J.C., and Cáceres, J.F. (2009). The SR protein family of splicing factors: master regulators of gene expression. *Biochem. J.* 417, 15–27.
- Mason, M.M., Heras, S.R., Bellora, N., Eyra, E., and Cáceres, J.F. (2014). The translational landscape of the splicing factor SRSF1 and its role in mitosis. *eLife* May 6, e02028.
- Michlewski, G., Sanford, J.R., and Cáceres, J.F. (2008). The splicing factor SF2/ASF regulates translation initiation by enhancing phosphorylation of 4E-BP1. *Mol. Cell* 30, 179–189.
- Mizuno, H., Kitada, K., Nakai, K., and Sarai, A. (2009). PrognoScan: a new database for meta-analysis of the prognostic value of genes. *BMC Med. Genomics* 2, 18.
- Müller-McNicoll, M., Botti, V., de Jesus Domingues, A.M., Brandl, H., Schwich, O.D., Steiner, M.C., Curk, T., Poser, I., Zarnack, K., and Neugebauer, K.M. (2016). SR proteins are NXF1 adaptors that link alternative RNA processing to mRNA export. *Genes Dev.* 30, 553–566.
- Muramatsu, T., Kozaki, K.I., Imoto, S., Yamaguchi, R., Tsuda, H., Kawano, T., Fujiwara, N., Morishita, M., Miyano, S., and Inazawa, J. (2016). The hypusine cascade promotes cancer progression and metastasis through the regulation of RhoA in squamous cell carcinoma. *Oncogene* 35, 5304–5316.
- Muthuswamy, S.K., Li, D., Lelievre, S., Bissell, M.J., and Brugge, J.S. (2001). ErbB2, but not ErbB1, reinitiates proliferation and induces luminal repopulation in epithelial acini. *Nat. Cell Biol.* 3, 785–792.
- Oran, A.R., Adams, C.M., Zhang, X.Y., Gennaro, V.J., Pfeiffer, H.K., Mellert, H.S., Seidel, H.E., Mascioli, K., Kaplan, J., Gaballa, M.R., et al. (2016). Multifocal control of mitochondrial gene expression by oncogenic MYC provides potential therapeutic targets in cancer. *Oncotarget* 7, 72395–72414.
- Pandit, S., Zhou, Y., Shiue, L., Coutinho-Mansfield, G., Li, H., Qiu, J., Huang, J., Yeo, G.W., Ares, M., Jr., and Fu, X.D. (2013). Genome-wide analysis reveals SR protein cooperation and competition in regulated splicing. *Mol. Cell* 50, 223–235.
- Partanen, J.I., Nieminen, A.I., Mäkelä, T.P., and Klefstrom, J. (2007). Suppression of oncogenic properties of c-Myc by LKB1-controlled epithelial organization. *Proc. Natl. Acad. Sci. USA* 104, 14694–14699.
- Pelisch, F., Khauv, D., Rizzo, G., Stallings-Mann, M., Blaustein, M., Quadrana, L., Radisky, D.C., and Srebrow, A. (2012). Involvement of hnRNP A1 in the matrix metalloproteinase-3-dependent regulation of Rac1 pre-mRNA splicing. *J. Cell. Biochem.* 113, 2319–2329.
- Pind, M.T., and Watson, P.H. (2003). SR protein expression and CD44 splicing pattern in human breast tumours. *Breast Cancer Res. Treat.* 79, 75–82.

- Pinke, D.E., and Lee, J.M. (2011). The lipid kinase PI4KIII $\beta$  and the eEF1A2 oncogene co-operate to disrupt three-dimensional *in vitro* acinar morphogenesis. *Exp. Cell Res.* 317, 2503–2511.
- Quinlan, A.R., and Hall, I.M. (2010). BEDTools: a flexible suite of utilities for comparing genomic features. *Bioinformatics* 26, 841–842.
- Reaves, D.K., Hoadley, K.A., Fagan-Solis, K.D., Jima, D.D., Bereman, M., Thorpe, L., Hicks, J., McDonald, D., Troester, M.A., Perou, C.M., and Fleming, J.M. (2017). Nuclear Localized LSR: A Novel Regulator of Breast Cancer Behavior and Tumorigenesis. *Mol. Cancer Res.* 15, 165–178.
- Reynolds, S.M., Miller, M., Lee, P., Leinonen, K., Paquette, S.M., Rodebaugh, Z., Hahn, A., Gibbs, D.L., Slagel, J., Longabaugh, W.J., et al. (2017). The ISB Cancer Genomics Cloud: A Flexible Cloud-Based Platform for Cancer Genomics Research. *Cancer Res.* 77, e7–e10.
- Sanford, J.R., Gray, N.K., Beckmann, K., and Cáceres, J.F. (2004). A novel role for shuttling SR proteins in mRNA translation. *Genes Dev.* 18, 755–768.
- Sanford, J.R., Coutinho, P., Hackett, J.A., Wang, X., Ranahan, W., and Cáceres, J.F. (2008). Identification of nuclear and cytoplasmic mRNA targets for the shuttling protein SF2/ASF. *PLoS One* 3, e3369.
- Sapra, A.K., Ankö, M.L., Grishina, I., Lorenz, M., Pabis, M., Poser, I., Rollins, J., Weiland, E.M., and Neugebauer, K.M. (2009). SR protein family members display diverse activities in the formation of nascent and mature mRNPs *in vivo*. *Mol. Cell* 34, 179–190.
- Sato, H., Hosoda, N., and Maquat, L.E. (2008). Efficiency of the pioneer round of translation affects the cellular site of nonsense-mediated mRNA decay. *Mol. Cell* 29, 255–262.
- Schneider, C.A., Rasband, W.S., and Eliceiri, K.W. (2012). NIH Image to ImageJ: 25 years of image analysis. *Nat. Methods* 9, 671–675.
- Shapiro, I.M., Cheng, A.W., Flytzanis, N.C., Balsamo, M., Condeelis, J.S., Oktay, M.H., Burge, C.B., and Gertler, F.B. (2011). An EMT-driven alternative splicing program occurs in human breast cancer and modulates cellular phenotype. *PLoS Genet.* 7, e1002218.
- Shen, S., Park, J.W., Lu, Z.X., Lin, L., Henry, M.D., Wu, Y.N., Zhou, Q., and Xing, Y. (2014). rMATS: robust and flexible detection of differential alternative splicing from replicate RNA-Seq data. *Proc. Natl. Acad. Sci. USA* 111, E5593–E5601.
- Stellzig, J., Chariot, A., Shostak, K., Ismail Göktuna, S., Renner, F., Acker, T., Pagenstecher, A., and Schmitz, M.L. (2013). Deregulated expression of TANK in glioblastomas triggers pro-tumorigenic ERK1/2 and AKT signaling pathways. *Oncogenesis* 2, e79.
- Stickeler, E., Kittrell, F., Medina, D., and Berget, S.M. (1999). Stage-specific changes in SR splicing factors and alternative splicing in mammary tumorigenesis. *Oncogene* 18, 3574–3582.
- Sun, X., Jin, Z., Song, X., Wang, J., Li, Y., Qian, X., Zhang, Y., and Yin, Y. (2015). Evaluation of KIF23 variant 1 expression and relevance as a novel prognostic factor in patients with hepatocellular carcinoma. *BMC Cancer* 15, 961.
- Swanson, C.M., Sherer, N.M., and Malim, M.H. (2010). SRp40 and SRp55 promote the translation of unspliced human immunodeficiency virus type 1 RNA. *J. Virol.* 84, 6748–6759.
- Swartz, J.E., Bor, Y.C., Misawa, Y., Rekosh, D., and Hammarskjöld, M.L. (2007). The shuttling SR protein 9G8 plays a role in translation of unspliced mRNA containing a constitutive transport element. *J. Biol. Chem.* 282, 19844–19853.
- The Cancer Genome Atlas Network (2012). Comprehensive molecular portraits of human breast tumours. *Nature* 490, 61–70.
- Trapnell, C., Roberts, A., Goff, L., Pertea, G., Kim, D., Kelley, D.R., Pimentel, H., Salzberg, S.L., Rinn, J.L., and Pachter, L. (2012). Differential gene and transcript expression analysis of RNA-seq experiments with TopHat and Cufflinks. *Nat. Protoc.* 7, 562–578.
- Trapnell, C., Hendrickson, D.G., Sauvageau, M., Goff, L., Rinn, J.L., and Pachter, L. (2013). Differential analysis of gene regulation at transcript resolution with RNA-seq. *Nat. Biotechnol.* 31, 46–53.
- Urbanski, L.M., Leclair, N., and Anczuków, O. (2018). Alternative-splicing defects in cancer: splicing regulators and their downstream targets, guiding the way to novel cancer therapeutics. *Wiley Interdiscip. Rev. RNA* 9, e1476.
- Venables, J.P., Klinck, R., Bramard, A., Inkel, L., Dufresne-Martin, G., Koh, C., Gervais-Bird, J., Lapointe, E., Froehlich, U., Durand, M., et al. (2008). Identification of alternative splicing markers for breast cancer. *Cancer Res.* 68, 9525–9531.
- Venables, J.P., Klinck, R., Koh, C., Gervais-Bird, J., Bramard, A., Inkel, L., Durand, M., Couture, S., Froehlich, U., Lapointe, E., et al. (2009). Cancer-associated regulation of alternative splicing. *Nat. Struct. Mol. Biol.* 16, 670–676.
- Wagner, S.D., Struck, A.J., Gupta, R., Farnsworth, D.R., Mahady, A.E., Eichinger, K., Thornton, C.A., Wang, E.T., and Berglund, J.A. (2016). Dose-Dependent Regulation of Alternative Splicing by MBNL Proteins Reveals Biomarkers for Myotonic Dystrophy. *PLoS Genet.* 12, e1006316.
- Wang, C., Norton, J.T., Ghosh, S., Kim, J., Fushimi, K., Wu, J.Y., Stack, M.S., and Huang, S. (2008). Polypyrimidine tract-binding protein (PTB) differentially affects malignancy in a cell line-dependent manner. *J. Biol. Chem.* 283, 20277–20287.
- Wang, X., Li, Y., Fan, Y., Yu, X., Mao, X., and Jin, F. (2018). PTBP1 promotes the growth of breast cancer cells through the PTEN/Akt pathway and autophagy. *J. Cell. Physiol.* 233, 8930–8939.
- Warzecha, C.C., Jiang, P., Amirikian, K., Dittmar, K.A., Lu, H., Shen, S., Guo, W., Xing, Y., and Carstens, R.P. (2010). An ESRP-regulated splicing programme is abrogated during the epithelial-mesenchymal transition. *EMBO J.* 29, 3286–3300.
- Watermann, D.O., Tang, Y., Zur Hausen, A., Jäger, M., Stamm, S., and Stickeler, E. (2006). Splicing factor Tra2-beta1 is specifically induced in breast cancer and regulates alternative splicing of the CD44 gene. *Cancer Res.* 66, 4774–4780.
- Weise, A., Bruser, K., Elfert, S., Wallmen, B., Wittel, Y., Wöhrle, S., and Hecht, A. (2010). Alternative splicing of Tcf7l2 transcripts generates protein variants with differential promoter-binding and transcriptional activation properties at Wnt/beta-catenin targets. *Nucleic Acids Res.* 38, 1964–1981.
- Wolter, P., Hanselmann, S., Pattschull, G., Schruf, E., and Gaubatz, S. (2017). Central spindle proteins and mitotic kinesins are direct transcriptional targets of MuvB, B-MYB and FOXM1 in breast cancer cell lines and are potential targets for therapy. *Oncotarget* 8, 11160–11172.
- Wu, J., Akerman, M., Sun, S., McCombie, W.R., Krainer, A.R., and Zhang, M.Q. (2011). SpliceTrap: a method to quantify alternative splicing under single cellular conditions. *Bioinformatics* 27, 3010–3016.
- Xiang, B., and Muthuswamy, S.K. (2006). Using three-dimensional acinar structures for molecular and cell biological assays. *Methods Enzymol.* 406, 692–701.
- Xu, Y., Gao, X.D., Lee, J.H., Huang, H., Tan, H., Ahn, J., Reinke, L.M., Peter, M.E., Feng, Y., Gius, D., et al. (2014). Cell type-restricted activity of hnRNPM promotes breast cancer metastasis via regulating alternative splicing. *Genes Dev.* 28, 1191–1203.
- Yamauchi, J., Miyamoto, Y., Chan, J.R., and Tanoue, A. (2008). ErbB2 directly activates the exchange factor Dock7 to promote Schwann cell migration. *J. Cell Biol.* 181, 351–365.
- Yap, C.S., Peterson, A.L., Castellani, G., Sedivy, J.M., and Neretti, N. (2011). Kinetic profiling of the c-Myc transcriptome and bioinformatic analysis of repressed gene promoters. *Cell Cycle* 10, 2184–2196.
- Yokoyama, Y., Matsumoto, A., Hieda, M., Shinchi, Y., Ogihara, E., Hamada, M., Nishioka, Y., Kimura, H., Yoshidome, K., Tsujimoto, M., and Matsuura, N. (2014). Loss of histone H4K20 trimethylation predicts poor prognosis in breast cancer and is associated with invasive activity. *Breast Cancer Res.* 16, R66.
- Yoshida, K., and Ogawa, S. (2014). Splicing factor mutations and cancer. *Wiley Interdiscip. Rev. RNA* 5, 445–459.
- Yoshino, H., Enokida, H., Chiyomaru, T., Tatarano, S., Hidaka, H., Yamasaki, T., Gotannda, T., Tachiwada, T., Nohata, N., Yamane, T., et al. (2012). Tumor suppressive microRNA-1 mediated novel apoptosis pathways through direct

- inhibition of splicing factor serine/arginine-rich 9 (SRSF9/SRp30c) in bladder cancer. *Biochem. Biophys. Res. Commun.* **417**, 588–593.
- Yu, M., Smolen, G.A., Zhang, J., Wittner, B., Schott, B.J., Brachtel, E., Ramaswamy, S., Maheswaran, S., and Haber, D.A. (2009). A developmentally regulated inducer of EMT, LBX1, contributes to breast cancer progression. *Genes Dev.* **23**, 1737–1742.
- Zahler, A.M., Neugebauer, K.M., Lane, W.S., and Roth, M.B. (1993). Distinct functions of SR proteins in alternative pre-mRNA splicing. *Science* **260**, 219–222.
- Zdobnov, E.M., and Apweiler, R. (2001). InterProScan—an integration platform for the signature-recognition methods in InterPro. *Bioinformatics* **17**, 847–848.
- Zhan, L., Rosenberg, A., Bergami, K.C., Yu, M., Xuan, Z., Jaffe, A.B., Allred, C., and Muthuswamy, S.K. (2008). Deregulation of scribble promotes mammary tumorigenesis and reveals a role for cell polarity in carcinoma. *Cell* **135**, 865–878.
- Zhang, Z., and Krainer, A.R. (2004). Involvement of SR proteins in mRNA surveillance. *Mol. Cell* **16**, 597–607.
- Zhu, J., and Krainer, A.R. (2000). Pre-mRNA splicing in the absence of an SR protein RS domain. *Genes Dev.* **14**, 3166–3178.
- Zuber, J., McJunkin, K., Fellmann, C., Dow, L.E., Taylor, M.J., Hannon, G.J., and Lowe, S.W. (2011). Toolkit for evaluating genes required for proliferation and survival using tetracycline-regulated RNAi. *Nat. Biotechnol.* **29**, 79–83.

## STAR★METHODS

### KEY RESOURCES TABLE

REAGENT or RESOURCE	SOURCE	IDENTIFIER
<b>Antibodies</b>		
Anti-T7 mouse	EMD Millipore	#69522-3; RRID: AB_11211744
Anti-cleaved caspase-3 rabbit	Cell Signaling	#9661L; RRID: AB_2341188
Anti-TRA2 $\beta$ rabbit	Abcam	#AB31353; RRID: AB_778565
Anti- $\beta$ Tubulin III rabbit	Genescript	#A01203-40; RRID: AB_1289179
anti-SRSF4	Bethyl Labs	#A303-670A; RRID: AB_11204752
anti SRSF6	CSHL antibody Facility	AK9-156
anti-SRSF9	CSHL antibody Facility	#AK251-24
Anti-ki67 rabbit	Zymed/ Invitrogen	#18-0191Z
Alexa Fluor 568 anti-mouse	Invitrogen	#A-11031; RRID: AB_144696
Alexa Fluor 488 anti-rabbit	Invitrogen	#A-11034; RRID: AB_2576217
IRDye 800CW Goat anti-Rabbit IgG (H + L)	Li-Cor	#926-32211; RRID: AB_621843
IRDye 680 Goat anti-Mouse IgG (H + L)	Li-Cor	#926-3220
<b>Chemicals, Peptides, and Recombinant Proteins</b>		
Matrigel Growth Factor Reduced	BD /Corning	#354230
Human Epithelial Growth Factor	Peptotech	#100-15
4-hydroxy-tamoxifen	Sigma	#H7904-5mg
Collagen	BD /Corning	#354236
Cell Recovery Solution	BD /Corning	#354253
Puromycin dihydrochloride	Sigma	#P8833
Hygromycin B	Sigma	#400053
G418	Goldbio	#G-418
Insulin	Sigma	#I-1882
D-luciferin, potassium salt	Goldbio	#LUCK-10 g
Doxycycline	RPI corporation	#D43020
Doxycycline food pellets	Harlan Teklad	#TD.05125
<b>Critical Commercial Assays</b>		
RNAeasy kit	QIAGEN	#74106
TrueSeq stranded mRNA Kit	Illumina	#RS-122-2101
iTaq Universal SYBR green Supermix	Bio-Rad	#172-5121
MTT assay	ATCC	# 30-1010K
<b>Deposited Data</b>		
RNA-seq MCF-10A	This paper	GSE137440
RNA-seq MDA-MB231	This paper	GSE137408
<b>Experimental Models: Cell Lines</b>		
MCF-10A	Laboratory of Senthil Muthuswamy	N/A
MDA-MB231	Laboratory of Min Yu	N/A
SUM159PT	Laboratory of Steve Ethier	N/A
<b>Recombinant DNA</b>		
PWZL-T7-SRSF1-Hygromycin	(Anczuków et al., 2012)	N/A
PWZL-T7-SRSF2-Hygromycin	This paper	N/A
PWZL-T7-SRSF3-Hygromycin	This paper	N/A
PWZL-T7-SRSF4-Hygromycin	This paper	N/A
PWZL-T7-SRSF6-Hygromycin	This paper	N/A

(Continued on next page)

**Continued**

REAGENT or RESOURCE	SOURCE	IDENTIFIER
PWZL-T7-SRSF9-Hygromycin	This paper	N/A
PWZL-T7-HNRNPA1-Hygromycin	This paper	N/A
PWZL-T7-TRA2B-Hygromycin	This paper	N/A
pBABE-MYC.ER-Puromycin	(Eilers et al., 1989)	N/A
TRMPV-Neo-SRSF4-sh1	This paper	N/A
TRMPV-Neo-SRSF4-sh2	This paper	N/A
TRMPV-Neo-SRSF6-sh1	This paper	N/A
TRMPV-Neo-SRSF6-sh2	This paper	N/A
TRMPV-Neo-SRSF9-sh1	This paper	N/A
TRMPV-Neo-SRSF9-sh2	This paper	N/A
TRMPV-Neo-TRA2B -sh1	This paper	N/A
TRMPV-Neo-TRA2B-sh2	This paper	N/A
TRMPV-Neo-HNRNPA1-sh1	This paper	N/A
TRMPV-Neo-HNRNPA1-sh2	This paper	N/A
TRMPV-Neo-control-sh1	This paper	N/A
rTTA3-Puro	(Zuber et al., 2011)	N/A
Sequence-Based Reagents		
shRNA sequence	This paper Table S7A	N/A
QPCR primer sequences	This paper Table S7B	N/A
RT-PCR primer sequences	This paper Table S7C	N/A
Software and Algorithms		
Cbio Portal	(Cerami et al., 2012)	<a href="http://www.cbioportal.org">www.cbioportal.org</a>
ISB-CGC	(Reynolds et al., 2017)	<a href="https://isb-cgc.appspot.com/">https://isb-cgc.appspot.com/</a>
dockerhub	N/A	<a href="https://hub.docker.com/">https://hub.docker.com/</a>
STAR v.2.5.1b	(Dobin et al., 2013)	<a href="https://github.com/alexdobin/STAR">https://github.com/alexdobin/STAR</a>
Cufflinks 2.2.1	(Trapnell et al., 2012)	<a href="http://cole-trapnell-lab.github.io/cufflinks/">http://cole-trapnell-lab.github.io/cufflinks/</a>
BedTools v.2.25.0	(Quinlan and Hall, 2010)	<a href="https://bedtools.readthedocs.io/en/latest/">https://bedtools.readthedocs.io/en/latest/</a>
Trimmomatic v.0.36	(Bolger et al., 2014)	<a href="http://www.usadellab.org/cms/?page=trimmomatic">http://www.usadellab.org/cms/?page=trimmomatic</a>
rMATS v.3.2.5	(Shen et al., 2014)	<a href="http://rnaseq-mats.sourceforge.net/">http://rnaseq-mats.sourceforge.net/</a>
enrichR	(Chen et al., 2013; Kuleshov et al., 2016)	<a href="https://cran.r-project.org/web/packages/enrichR/vignettes/enrichR.html">https://cran.r-project.org/web/packages/enrichR/vignettes/enrichR.html</a>
SpliceCore®	Envisagenics	<a href="https://www.envisagenics.com/platform/">https://www.envisagenics.com/platform/</a>
Prognoscan database	(Mizuno et al., 2009)	<a href="http://gibk21.bse.kyutech.ac.jp/ProгноScan/index.html">http://gibk21.bse.kyutech.ac.jp/ProгноScan/index.html</a>
Axiovision Digital Image Processing Software	Carl Zeiss	N/A
GraphPad Prism	GraphPad	N/A
ImageJ Digital Image Processing Software	(Schneider et al., 2012)	<a href="https://imagej.nih.gov/ij/">https://imagej.nih.gov/ij/</a>
Photoshop and Illustrator CC2018	Adobe	N/A

**LEAD CONTACT AND MATERIALS AVAILABILITY**

Further information and requests for resources and reagents should be directed to and will be fulfilled by the Lead Contact, Olga Anczukow ([olga.anczukow@jax.org](mailto:olga.anczukow@jax.org)).

Plasmid and cell lines generated are available from the Lead Contact without restrictions, with reasonable compensation by requestor for shipping. Request for access to the SpliceCore software platform may be submitted to Envisagenics. Access to SpliceCore will be governed by the terms of a negotiated agreement.

## EXPERIMENTAL MODEL AND SUBJECT DETAILS

### Human Cell Lines

Human mammary epithelial MCF-10A cells were obtained from the laboratory of Senthil K. Muthuswamy (Cold Spring Harbor Laboratory) and were maintained as described in DMEM/F12 supplemented with 5% horse serum, 20 ng/ml EGF (Peprotech), 0.5 mg/ml hydrocortisone (Sigma), 100 ng/ml cholera toxin (Sigma), 10  $\mu$ g/ml insulin (Sigma) and 1% penicillin streptomycin (Sigma) (Debnath et al., 2003a). Breast cancer cells lines, MDA-MB231-luciferase-GFP and SUM159PT were obtained from the laboratories of Min Yun (University of Southern California), and Steve Ethier (University of Southern California) respectively. MDA-MB231-luciferase-GFP cells were maintained as described (Yu et al., 2009). SUM-159PT were maintained in Ham's F-12 (Sigma) supplemented with 5% FBS, 1% penicillin streptomycin (Sigma), 5  $\mu$ g/ml insulin (Sigma) and 1  $\mu$ g/ml hydrocortisone (Sigma). Cells were grown at 37°C under a humidified atmosphere with 5% CO<sub>2</sub>. Cells were routinely authenticated by STR profiling, tested negative for mycoplasma using the MycoAlert Mycoplasma Detection Kit (Lonza), and cell aliquots from early passages were used. All cell lines used here were established from female subjects.

### Mice

NOD.Cg-Prkdcscid Il2rgtm1Wjl/SzJ female mice were obtained from The Jackson Laboratory and housed in Cold Spring Harbor Laboratory facilities. All mice used in these studies were female. Mice were group housed under a 12:12 light/dark cycle with access to food and water *ad libitum*. All animals were handled in accordance with Cold Spring Harbor Laboratory IACUC and AAALAC approved protocols and other ethics guidelines.

## METHOD DETAILS

### Plasmids

T7-tagged SRSF2, SRSF3, SRSF4, SRSF6, SRSF9, HNRNPA1 and TRA2 $\beta$  cDNA were subcloned from pcGT plasmids (Cáceres et al., 1997) into a pWZL-Hygro retroviral vector (a gift from S. Lowe, Cold Spring Harbor Laboratory) as described (Anczuków et al., 2012). PWZL-T7-SRSF1 (Anczuków et al., 2012) and pBabe-Puro-MYC.ER (Eilers et al., 1989) were described previously. SF-targeting shRNAs were designed using DSIR and sensor rules (Table S7A), and were cloned into TRMPV-Neo retroviral doxycycline-inducible shRNA expression vectors as described (Zuber et al., 2011). All vectors and inserts were verified and authenticated by Sanger sequencing.

### Cell Culture and Cell Lines

Populations of MCF-10A cells expressing either T7-tagged SRSF1, SRSF2, SRSF3, SRSF4, SRSF6, SRSF9, HNRNPA1 or TRA2 $\beta$  cDNA, with or without MYC.ER overexpression, were generated by retroviral transduction and selection with 2 $\mu$ g/ml puromycin or 200  $\mu$ g/ml hygromycin as described (Anczuków et al., 2012). Population of MDA-MB231-luciferase-GFP or SUM-159PT cells expressing rTTA3-puro and SF-shRNA-TRMPV-Neo were generated by retroviral transduction and selection with 2 $\mu$ g/ml puromycin or 1mg/ml G418 as described (Zuber et al., 2011).

### Three-Dimensional Morphogenesis Assay

MCF-10A or MDA-MB231 stable cell lines were seeded on an 8-well glass chamber slide coated with Matrigel Growth Factor Reduced (BD Biosciences) as described (Debnath et al., 2003a) at a density of 5,000 cells per well and maintained in their respective media. At least 100 acini or structures were imaged at indicated time points using a Zeiss Axiovert 200M microscope and AxioVision 4.5 software (Zeiss). MYC.ER acini were stimulated with 1  $\mu$ M 4-hydroxy-tamoxifen (Sigma) on day 3, and the medium with inducer was replaced every 3 days, as described (Zhan et al., 2008). For shRNA induction, MDA-MB231 or SUM159PT cell media was supplemented with 1–2  $\mu$ g ml<sup>-1</sup> doxycycline at the indicated time points, and the media was replaced every 3 days. For high-content imaging of 3D structures, 6,000 MDA-MB231 or 8,000 SUM159PT cells were plated per well in 48-well plates, and fluorescent images were acquired using a high-content imaging Opera Phoenix instrument (Perkin Elmer) and assembled using the Harmony software (Perkin Elmer) as a maximum projection image composed of 30–35 Z stack images taken every 55  $\mu$ m. For downstream RNA or protein extraction from 3D cultured MCF-10A or MDA-MB231 cells were washed with PBS, and Matrigel was dissolved by incubating slides at 4°C in Cell Recovery Solution (BD).

### Immunofluorescence

All procedures were performed as described (Anczuków et al., 2012). Microscopy was performed on a Zeiss Axiovert 200M instrument using the ApoTome imaging system (Zeiss) or the Dragonfly Spinning Disk system (Andor). T7 (CSHL antibody facility), cleaved caspase-3 (Cell Signaling) and ki67 (Zymed) primary antibodies were used at 1/50, 1/100 and 1/100 dilutions, respectively. Alexa Fluor 568 anti-mouse and 488 anti-rabbit secondary antibodies (Invitrogen) were used at 1/500 dilution. Acini were scored positive for ki67 when at least five cells within the acini were stained and positive for cleaved caspase-3 when at least one cell in the lumen was stained.

### Quantitative RT-PCR Analysis

3D cultured MCF-10A cells were harvested as described above and RNA was extracted using an RNAeasy kit (QIAGEN) including DNase I treatment. 1  $\mu$ g of RNA was reverse-transcribed with Superscript III reverse transcriptase (Invitrogen). QPCR was used to amplify endogenous transcripts with the SF-specific primers listed in [Table S7B](#) using cDNA corresponding to 5ng of RNA. QPCR was performed with iTaq Universal SYBR green Supermix (Bio-Rad) in 384-well plates (Life Technologies) using a ViiA7 Real-Time PCR system (Life Technologies) per manufacturer instructions. Results were analyzed with QuantStudio Real-Time PCR software, and SF expression was normalized to housekeeping genes *GAPDH* and *HPRT*.

### Western Blot Analysis

Cells were lysed in Laemmli buffer (50 mM Tris-HCl pH 6.2, 5% (v/v)  $\beta$ -mercaptoethanol, 10% (v/v) glycerol, 3% (w/v) SDS). Equal amounts of total protein were loaded on a 12% SDS-polyacrylamide gel, transferred onto a nitrocellulose membrane (Millipore) and blocked in 5% (w/v) milk in Tween 20-TBST (50 mM Tris pH 7.5, 150 mM NaCl, 0.05% (v/v) Tween 20). Blots were incubated with anti-T7 (EMD Millipore #69522-3), anti-SRSF4 (Bethyl Laboratories #A303-670A), anti SRSF6 (CSHL antibody facility AK9-156), anti-SRSF9 (CSHL antibody facility #AK251-24), anti-TRA2B (Abcam #ab31353), or anti- $\beta$  Tubulin III (Genescript #A01203-40) primary antibodies. IR-Dye 680 anti-mouse or IR-Dye 800 anti-rabbit immunoglobulin G (IgG) secondary antibodies (LI-COR) were used for infrared detection and quantification with an Odyssey imaging system (LI-COR).

### RNA-Sequencing Library Preparation

3D cultured MCF-10A or MDA-MB231 cells were harvested as described above and total RNA was extracted using an RNAeasy kit (QIAGEN) including DNase I treatment. RNA libraries were prepared and barcoded using a TrueSeq stranded mRNA kit with polyA selection (Illumina), and quantified using a Bioanalyzer DNA 1000 chip (Agilent). Equal amounts of libraries were pooled (3 libraries per lane) and sequenced as 101bp (MCF-10A) or 150bp (MDA-MB231) paired-ended reads on an Illumina HiSeq instrument at >80-100 million reads per library. At least 3 independent libraries were generated for each experimental condition.

### RT-PCR Splicing Event Validation

MCF-10A, MDA-MB231 or SUM159PT cells were harvested as described above and RNA was extracted using an RNAeasy kit (QIAGEN) including DNase I treatment. 1  $\mu$ g of total RNA was reverse-transcribed with Superscript III reverse transcriptase (Invitrogen). Semiquantitative PCR was used to amplify endogenous transcripts with the primers listed in [Table S7C](#) with cDNA from 5-20ng of RNA. Optimal PCR conditions were defined for each primer pair by testing amplification from 26-30 cycles to select semiquantitative conditions. PCR products were separated by 2% agarose gel stained with SYBRsafe (Invitrogen), and bands were quantified with a ChemiDoc MP Imaging System (Bio-Rad). The ratio of each isoform was first normalized to the sum of the different isoforms, and changes were then expressed as the fold increase compared to the levels obtained for cells or acini expressing the control vector.

### Wound-Healing Assays

250,000 MCF-10A or 100,000 MDA-MB231 cells were grown in 6-well plates for 48 hours. For shRNA induction, the media was supplemented with 2  $\mu$  ml<sup>-1</sup> doxycycline at 24 hours before the start of the experiment and maintained until the end. A scratch was performed in the confluent monolayer with a P200 tip and the wells were washed twice with media. The same field was imaged with a Zeiss Observer microscope at 0h and 16h after induction of the wound. The size of the gap was measured using the Axiovision digital image processing software (Zeiss).

### Transwell Migration Assays

150,000 MCF-10A or 25,000 MDA-MB231 cells in serum-free media were seeded on top of an 8- $\mu$ m PET membrane transwell (BD Biosciences) in a 24-well format and allowed to migrate into the lower compartment containing complete media with serum and growth factors for 16 or 4 hours for MCF-10A or MDA-MB231 cells, respectively. For shRNA induction, the media was supplemented with 2  $\mu$  ml<sup>-1</sup> doxycycline at 24 hours before the start of the experiment and maintained until the end. After removal of the cells on top of the filter, the remaining cells were fixed with 5% formalin, permeabilized with 0.5% Triton X-100 and stained with DAPI. DAPI-positive nuclei were imaged using a Zeiss Observer microscope, and counted using the ImageJ digital image processing software.

### 3D Invasion Assays

Collagen-matrigel invasion assays were performed as described ([Xiang and Muthuswamy, 2006](#)). Briefly, 5,000 MCF-10A cells were seeded on a 1:2 mix of collagen:Matrigel in 8-well glass slide chamber. Media was replaced every 4 days, and acini were imaged at day-8 and day-16 using a Zeiss Observer microscope.

### MTT Assay

Cell proliferation assays were performed with an ATCC MTT Assay kit (ATCC). Briefly 2,000 MDA-MB231 cells were plated into 96-well plates in triplicates in cell growth media with or without doxycycline. Cells were grown for 1-4 days and stained with the MTT reagent as recommended by the manufacturer. Wavelength was read on a SpectraMax M plate reader.

### In Vivo Metastasis Modeling

Animal experiments were carried out in the Cold Spring Harbor Laboratory Animal Shared Resource in accordance with Cold Spring Harbor Laboratory Institutional Animal Care and Use Committee-approved procedures.  $0.5\text{-}1 \times 10^6$  MDA-MB231-luciferase-GFP control or TRA2 $\beta$  shRNA inducible cells were injected either into the tail vein or into the mammary fat pad of 8-week-old NOD.Cg-Prkdc<sup>scid</sup> Il2rg<sup>tm1Wjl/SzJ</sup> (The Jackson Laboratory #5557) female mice. For shRNA induction, half of the mice were treated with doxycycline in both drinking water (1.5 mg ml<sup>-1</sup> with 2% sucrose; RPI Corporation and Sigma-Aldrich) and food (625 mg kg<sup>-1</sup>, Harlan Laboratories). Doxycycline water was replaced every 3 days. Whole-body bioluminescent imaging was performed using an IVIS100 system (Caliper LifeSciences) as described (Zuber et al., 2011). Briefly, primary tumor growth and metastasis formation were monitored every 3-4 days by bioluminescence imaging following intraperitoneal injection of D-Luciferin (25 mg kg<sup>-1</sup>, Goldbio). Animal weight and primary tumor size was recorded bi-weekly. Animals were euthanized 50-60 days post-injection by cardiac perfusion of a 4% paraformaldehyde (PFA) solution. Primary tumors were collected and flash-frozen for RNA and protein extraction, or fixed in 4% PFA, washed with PBS, embedded in paraffin, sectioned, and stained with hematoxylin & eosin. Following a detailed necropsy, lung and liver tissues were fixed in 4% PFA, cryo-protected in sucrose gradient, embedded in OCT solution (Tissue-Tek) and frozen. Serial transversal sections of lung and liver were then performed through the whole tissue, every 2mm, and were re-embedded horizontally to obtain serial sections of the entire organ, and frozen in fresh OCT. Lung and liver sections were staining with hematoxylin & eosin and slides were imaged using an Aperio slide scanner (Leica). Micro- and macro-metastasis areas were then quantified relative to the whole organ area using an Aperio Scanscope (Leica).

### Differential Splicing Analysis

We used the SpliceCore® software platform (<https://www.envisagenics.com/platform/>) to identify cancer-related differential splicing events (DSEs). SpliceCore is operated through a user interface built on the Microsoft Azure cloud to facilitate data trafficking, storage, HIPAA compliance and compute scalability. To identify DSEs changes co-occurring in cancer, SpliceCore utilizes a reference database called TXdb<sup>TM</sup>, which incorporates over 5M exon-trio models (Wu et al., 2011) derived from the entire TCGA database, including ~1.5K breast cancer datasets. To prioritize reproducible DSEs, we complemented SpliceCore with additional in-house data analysis. Our in-house pipeline implemented STAR (v.2.5.1b) (Dobin et al., 2013), Cufflinks Suite (v.2.2.1) (Trapnell et al., 2012) and rMATS (v.3.2.5) (Shen et al., 2014). Paired-end reads were preprocessed for trimming of low-quality regions by Trimmomatic (v. 0.36) (Bolger et al., 2014) and mapped to the human reference genome using STAR in 2-pass mode with the Gencode GRCh37 v.25 reference transcript annotation. To include novel exons and introns in the analysis, we also performed an annotation-guided transcriptome reconstruction and merged the resulting transcriptome from each sample into a comprehensive transcript annotation (GTF) with Cufflinks and Cuffmerge (Cufflinks suites v.2.2.1) (Trapnell et al., 2012) using the “-multi-read-correct” and “-library-type fr-first-strand” (strand-specific library for dUTP protocol) parameters. Each RNA-seq replicate was processed independently in SpliceCore and in-house to produce individual “percent spliced in” (PSI) scores. In this manner we increased the sensitivity of the analysis by ensuring a larger number of AS events to be detected by at least one method. Next, we integrated both SpliceCore’s and in-house individual PSI scores to compute DSEs as “differential percent spliced in” ( $\Delta$ PSI) scores. Global  $\Delta$ PSI scores were estimated as the difference of the mean PSIs detected across RNA-seq replicates by at least one method:  $\Delta\text{PSI}^{\text{global}} = \text{mean}(\text{PSI}^{\text{case}}) - \text{mean}(\text{PSI}^{\text{control}})$ . To eliminate inconsistent results, we performed a quality control whereby we estimated individual  $\Delta$ PSIs for each “*i*”, where “*i*”s are the list of all case datasets analyzed by every method. For each “*i*” we estimated individual  $\Delta\text{PSI}^i = \text{PSI}^i - \text{mean}(\text{PSI}^{\text{control}})$ . If the sign of the geometric mean of all “ $\text{sgn}(\prod_{i=1}^n \Delta\text{PSI}_i)$ ” did not equal  $\text{sgn}(\Delta\text{PSI}^{\text{global}})$  then the splicing event was called inconsistent and filtered out. For each analyzed dataset (i.e., TCGA, MCF-10A and MDA-MB231) we applied further filtering criteria explained below.

### TCGA Data Analysis

The RNA-seq data from TCGA breast tumors were retrieved and processed on the ISB Cancer Genomics Cloud Platform (<https://isb-cgc.appspot.com/>). Sample IDs are listed in Table S2A.

CNVs and expression changes in SFs were assessed by DNA- and RNA-seq, respectively, from a collection of human breast tumors from The Cancer Genome Atlas (TCGA) dataset (n = 960) (The Cancer Genome Atlas Network, 2012) as described previously (Cerami et al., 2012; Gao et al., 2013). Graphical OncoPrint representations were generated using the Cbio portal (<http://www.cbioportal.org/>) for all breast tumors, as well as for samples annotated as triple negative breast tumors. Pre-computed Z-score and clinical information, e.g., PAM50 signatures, were retrieved from Cbio for downstream analysis.

Human TCGA breast tumors (n = 960) (The Cancer Genome Atlas Network, 2012) were classified into *SF-low* (Z-score  $\leq 0$ ) or *SF-high* (Z-score  $\geq 1.5$ ) tumors according to their SF expression for *SRSF1*, *SRSF2*, *SRSF3*, *SRSF4*, *SRSF5*, *SRSF6*, *SRSF7*, *SRSF8*, *SRSF9*, *SRSF10*, *SRSF11*, *SRSF12*, *TRA2 $\beta$*  and *HNRNPA1* using pre-computed Z-score values from cBioPortal (<http://www.cbioportal.org/>) (Cerami et al., 2012; Gao et al., 2013) (Table S2A). Splicing events were defined using both splice junction read counts and alternatively spliced exon body counts for each event to calculate a PSI score for each local event, as well as a  $\Delta$ PSI in *SF<sup>low</sup>* versus *SF<sup>high</sup>* tumors using SpliceCore and in-house methods as described above. The in-house pipeline was implemented using corresponding dockers (<https://www.docker.com/products/docker-hub>) on a cloud instance. Significant DSEs were selected as follows: i)  $\Delta\text{PSI} = |\text{mean PSI } SF^{\text{high}} - \text{mean PSI } SF^{\text{low}}| \geq 0.1$ ; and ii)  $\text{FDR} \leq 0.05$ ; and iii) at least an average of 5 reads per dataset detected in both *SF<sup>low</sup>* and *SF<sup>high</sup>* tumors that support either exon skipping or inclusion, i.e., (inclusion count  $> 5$  in either control

OR case) AND (skipping count  $> = 5$  in either control OR case). To correct for missing data due to sequencing depth below 100 million reads per sample in the TCGA dataset, we focused only on DSEs detected in at least 10 tumors from both groups.

### Differential Splicing Analysis of MCF-10A and MDA-MB231 Cell Lines

DSEs between two groups, such as control *versus* SF-OE/KD, were determined using SpliceCore and in-house methods as described above. Significant DSEs were selected as follows: i)  $\Delta\text{PSI} = |\text{mean PSI}^{\text{SF-OE/KD}} - \text{mean PSI}^{\text{control}}| \geq 0.1$ ; and ii)  $\text{FDR} \leq 0.05$ ; and iii) at least 5 reads (averaged across all biological replicates) detected in both the control and SF-OE/KD that support either exon skipping or inclusion, i.e., (inclusion count  $> = 5$  in either control OR case) AND (skipping count  $> = 5$  in either control OR case). For MDA-MB231 cells, the significant DSEs from TRA2 $\beta$ sh +DOX *versus* -DOX were discarded if they also appeared as significant and altered in the same direction in CTLsh +DOX *versus* -DOX cells.

### Pairwise Comparison of DSEs Across Multiple Studies

To compare the overlap in DSEs between two studies, A and B, we performed a Fisher's exact test (with 'two-sided' test to the null hypothesis) in which: i) DA and DB are all the detected AS events in study A or study B, respectively; ii) SA and SB are the statistically significant DSEs detected in study A or study B, respectively ( $|\Delta\text{PSI}| \geq 0.1$ ;  $\text{FDR} \leq 0.05$ ;  $\geq 5$  reads averaged across all replicates); iii) the intersection of significant DSEs with  $\Delta\text{PSI}$  in the same direction (i.e., either both  $\geq 0.1$  or both  $\leq -0.1$ ) is defined as  $iS = SA \& SB$ ; and iv) the total splicing "universe" is defined by the union of splicing events as  $D = DA \cup DB$ . Thus, the strength of overlap of DSEs in two studies is calculated using a Fisher's exact test computed from the following 2x2 contingency table, along with odds ratio and  $P$ -values.

	inA	notA
inB	iS	B - iS
notB	A - iS	D - iS

To compare the similarity in DSEs between two studies, the Jaccard similarity index is calculated as  $J = SA \& SB / SA \cup SB$ . The analysis was conducted either on splicing events (DSEs) or one genes that exhibit at least one DSE (DSGs).  $P$ -values were corrected using Bonferroni's method.

### Differential Gene Expression Analysis

Preprocessing of reads and mapping steps was performed as mentioned for the differential splicing analysis. Using mapped files (BAM), differential expression of annotated genes (Gencode GRCh37) in control *versus* SF-OE/KD was determined with Cuffdiff (v.2.2.1) (Trapnell et al., 2012) using the "-multi-read-correct" and "-library-type fr-firststrand" (strand-specific library) parameters. Significant genes were selected as follows: i)  $\text{FDR} \leq 0.05$ ; ii)  $|\log_2 \text{fold change}| \geq 0.3$ ; and iii) test status = "OK." For MDA-MB231 cells, genes with significant differential expression in TRA2 $\beta$ sh +DOX *versus* -DOX were discarded, if they also appeared as significant and altered in the same direction in CTLsh +DOX *versus* -DOX cells.

### Protein Domain Annotation

Proteins domain were annotated using the InterProScan Pfam predictive module (Zdobnov and Apweiler, 2001). SpliceCore's exon trios were translated to protein in three different reading frames and the optimal one was chosen for domain annotation. Optimal reading frames were selected based on alignment score to known protein sequences expressed from the coding locus.

### Annotation of Genes with Breast Cancer Relevance

Genes associated with breast carcinoma based on GWAS, functional genomics, and literature data mining were retrieved from the Open Targets Platform (<https://www.opentargets.org/>).

### Gene Enrichment Analysis

Gene enrichment analysis was performed using a Bioconductor package, enrichR (Chen et al., 2013; Kuleshov et al., 2016) for both i) genes that exhibit altered splicing (significant DSEs), ii) genes that exhibit differential splicing (DSGs), and iii) genes that exhibit changes in expression in SF-OE *versus* control MCF-10A cells or SF-KD *versus* control MDA-MB231 cells. We reported the top 100 enriched targets sorted based on FDR.

### MYC and TRA2 $\beta$ Association Analysis

MYC and TRA2 $\beta$  amplification status and expression were calculated using the Cbio portal (<http://www.cbioportal.org/>) for human tumor RNA-seq data from The Cancer Genome Atlas Project as described (Cerami et al., 2012; Gao et al., 2013) or using microarray data from GEO GSE2109 (<https://www.ncbi.nlm.nih.gov/projects/geo/query/acc.cgi?acc=GSE2109>) as described (Anczuków et al., 2012). The association between MYC and TRA2 $\beta$  was computed using a two-tailed Fisher's exact test and corrected for multiple testing.

### MYC Binding Data

MYC ChIP-seq datasets from MCF-7 (ENCSR000DMJ) and MCF-10A (ENCSR000DOS) cells were analyzed as described on <https://www.encodeproject.org/> and visualized using <http://genome.ucsc.edu>. Plotted tracks are fold changes over controls for pooled replicates, as well as representative ChIP-seq peaks called using conservative IDR thresholds.

### TRA2 $\beta$ Expression and Clinical Outcome Analysis

Patients were stratified in *TRA2 $\beta$ -high* or *-low* expression groups using the minimum *P*-value approach as described (Mizuno et al., 2009). Correlations between *TRA2 $\beta$*  expression and overall survival or distant-metastasis-free-survival for multiple breast cancer patient cohorts were retrieved from the Prognoscan database (Mizuno et al., 2009) (<http://gibk21.bse.kyutech.ac.jp/PrognoScan/index.html>).

### Graphs and Figures

Graphs were generated using GraphPad Prism 5 software. Figures were generated using Adobe CC 2018 Photoshop and Illustrator software in compliance with the Nature Publishing Group policy concerning image integrity.

### QUANTIFICATION AND STATISTICAL ANALYSIS

Where appropriate, the data are presented as the mean  $\pm$  s.d., as indicated. Data points were compared using an unpaired two-tailed Student *t* test or two-tailed Mann-Whitney test, as indicated in the legends. For quantification of proliferation and apoptosis markers, a two-tailed Fisher test was used. A Mantel-Cox test was used to compare tumor-free survival of mice in the transplantation experiment. *P*-values are indicated in the figure legends.

### DATA AND CODE AVAILABILITY

The accession numbers for RNA-sequencing data are GEO: GSE137440 (RNA-seq MCF-10A) and GSE137408 (RNA-seq MDA-MB231).

RNA-sequencing data from TCGA breast tumors (The Cancer Genome Atlas Network, 2012) is available via ISB-CGC cloud. Sample IDs are listed in Table S2A. ChIP-seq datasets (ENCSR000DMJ and ENCSR000DOS) are available from <https://www.encodeproject.org/>.